ANALYSIS OF SUBHARMONIC OSCILLATIONS IN EXTRA-HIGH-VOLTAGE EXTRA-LONG-DISTANCE TRANSMISSION LINES

A Thesis

Presented to

the Faculty of Graduate Studies and Research

The University of Manitoba

In Partial Fulfillment

of the Requirements for the Degree

Master of Science in Electrical Engineering.

by

KONG-WAI KAN

May 1969

TO MY MOTHER

ABSTRACT

This thesis is concerned with the problem of predicting the subharmonic oscillations in a compensated extra-high-voltage extra-long-distance transmission line. A mathematical analysis and an analogue computer simulation are described. Under switching and unbalanced fault conditions, the results obtained by the analogue computer illustrate the hazard of subharmonic oscillations in extra-high-voltage extra-long-distance (EHV ELD) transmission lines, where both series and shunt compensations are considered.

ACKNOWLEDGEMENT

The author is indebted to Professor M. Z. Tarnawecky, and Dr. G. W. Swift for their original suggestions, guidance and assistance in the preparation of this thesis. Thanks are also due to the National Research Council, Ottawa, who provided the financial aid to enable the author to carry out this study.

TABLE OF CONTENTS

LIST OF FIGURES

LIST OF TABLES

INTRODUCTION

The use of both series and shunt compensations to increase power transfer, reliability and stability in extra-high-voltage extra-long-distance (EHV ELD) transmission lines results in a non-linear circuit* with the inherent line resistance and line inductance, which gives rise to abnormal over-voltages. The difficulties encountered in any attempt to analyse mathematically the behaviour of this non-linear circuit arise from the fact that superposition is no longer valid in analysing the differential equation of a non-linear circuit. The reason for this is that in linear circuits the transient dies out as time goes on, so that after sufficient time has elapsed, only the steady state remains as the sole solution for the differential equation of the linear circuit. However, in non-linear circuits, the transient component will persist and together with the steady state component form the total solution for the differential equation of the non-linear circuit.**

The purpose of this study is to introduce effective techniques available for the analysis of subharmonic oscillations and to answer the following questions:

(a) What are the subharmonic oscillations and how do they occur?

(b) Is high series compensation level more susceptible to subharmonic oscillations?

---

* See Appendix A. Page 63.

** See Chapter IV, Mathematical Analysis.

(c) What is the magnitude of the line current and capacitor voltage at subharmonic resonance?

(d) How can these subharmonic oscillations be controlled or eliminated?

CHAPTER I

ANALYSIS OF CIRCUIT ELEMENTS AND HYSTERESIS

The introduction of a non-linear element in conjunction with other linear elements in the circuit may eliminate the possibility of a simple analysis for the system. In order to analyse the nonlinear response, it is necessary to become familiar with the non-linear element or elements in the circuit under study. The equivalent circuit of the EHV ELD transmission line that is of particular interest to the author, contains line resistance, line inductance, series capacitance and non-linear inductance. (See Figure 4.1(a), Page 33). The investigations are as follows:

I.1 Linear Elements.

The linear elements in the circuit under study are: line resistance, line inductance and series capacitance.

I.1.1 Resistance.

A German physicist, George Simon Ohm, found that the current was directly proportional to the voltage for a given material. The proportionality constant was a function of the particular material and geometric sample The mathematical expression is:

$$V_r \propto I_r \tag{1.1}$$

that is:

$$V_r = I_r R \tag{1.2}$$

where R is a constant and is defined as a resistance

I_r is the current through the resistance

V_r is the voltage across the resistance.

Equation (1.2) is known as Ohm's Law. If the characteristic of a resistance obeys Ohm's law, it is a linear resistance. If Ohm's law does not apply it is a non-linear resistance. The characteristics of the linear and non-linear resistances are shown in Fig. 1.1

I.1.2 Inductance

The time rate of change of flux linkages produced as a result of the movement of a coil with respect to a magnetic field , causes an induced voltage V_i according to the equation:

$$V_i = \frac{d\psi}{dt} \tag{1.3}$$

where ψ is the total flux linkages expressed in webers.

In particular, if the flux linkages are produced by a current flowing through the coil, Equation (1.3) can be written as:

$$V_i = \frac{d\psi}{di} \cdot \frac{di}{dt} \tag{1.4}$$

If the flux linkages are linearly proportional to the current, then:

$$\frac{d\psi}{di} = \frac{\psi}{i} = L \tag{1.5}$$

where L is a constant and defined as the inductance of the coil, expressed in henrys.

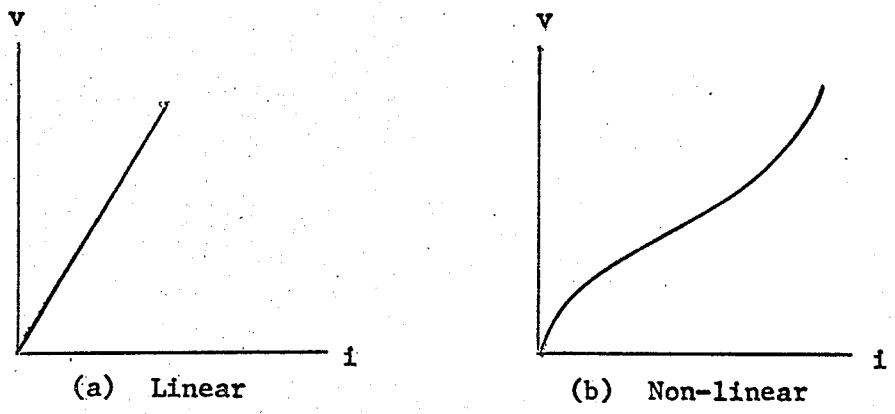

(a) Linear (b) Non-linear

FIGURE 1.1 Characteristics of Resistances.

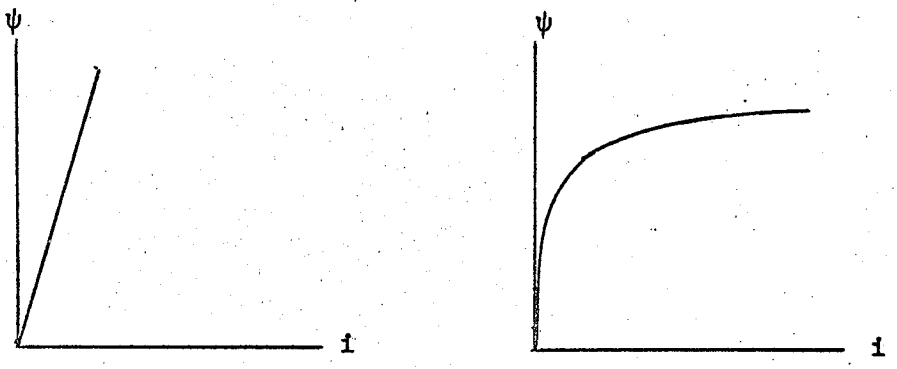

(a) Linear (b) Non-linear

FIGURE 1.2 Characteristics of Inductances

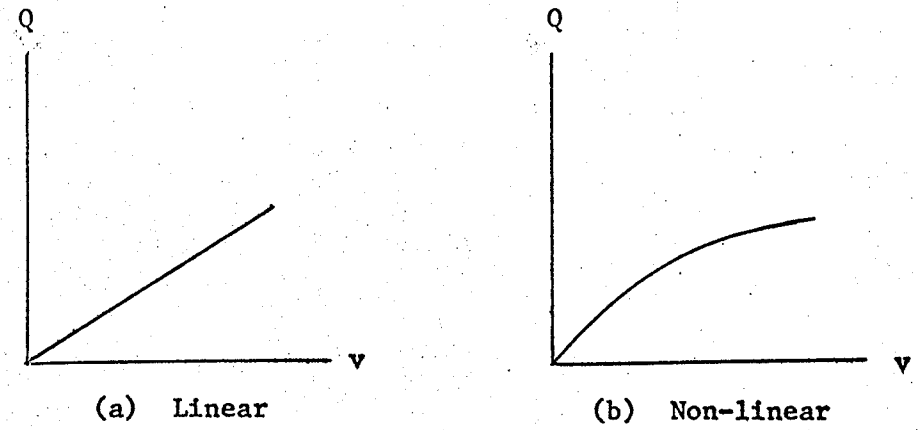

(a) Linear (b) Non-linear

FIGURE 1.3 Characteristics of Capacitances.

Substituting Equation (1.5) into Equation (1.4) yields:

$$V_i = L \frac{di}{dt} \tag{1.6}$$

The induced voltage expressed in Equation (1.6) is valid if the inductance is linear. (See Figure 1.2)

I.1.3 Capacitance.

Mathematically, we may express the relationship for a linear capacitance as:

$$C = \frac{Q}{V_c} \tag{1.7}$$

where V_c is the voltage across the capacitor

Q is the charge on the capacitor expressed in coulombs

C is a constant and is defined as the capacitance expressed in farads.

In addition to equation (1.7), capacitance can also be expressed as:

$$C = \frac{\varepsilon A}{d_c} \tag{1.8}$$

where A is the area of the capacitor

d_c is the spacing between the two plates of the capacitor

ε is the permittivity of the linear dielectric of the capacitor.

Neither Equation (1.7) nor Equation (1.8) is valid if the capacitance is non-linear. The characteristics of the linear and non-linear capacitances are shown in Fig. 1.3.

I.2 Non-linear element.

The shunt reactor is the only non-linear element in the circuit under study. Due to the properties of the magnetic material the inductance of a shunt reactor is non-linear.

I.2.1 Non-linear inductance.

The permeability of magnetic materials such as iron, steel, and nickel-iron varies with the flux density. A typical $i - \psi$ characteristic curve is shown in Fig. 1.2.

A study of the $i - \psi$ non-linear characteristic curve reveals that the flux linkages are no longer linearly proportional to the current. Equation (1.6) is not valid in expressing non-linear inductance since:

$$\frac{d\psi}{di} = L(i) \tag{1.9}$$

where $L(i)$ is the non-linear inductance which varies with the current Substituting Equation (1.9) into Equation (1.4) yields:

$$V_i = L(i) \frac{di}{dt} \tag{1.10}$$

In the analysis of the nonlinear response it has been found that it is more convenient to express the non-linear induced voltage as in Equation (1.3) rather than Equation (1.10).

It should be noted however, that the characteristic curve of a magnetic material is not a single curve but a whole family of curves. The neutral curve and the number of closed hysteresis loops of low and medium

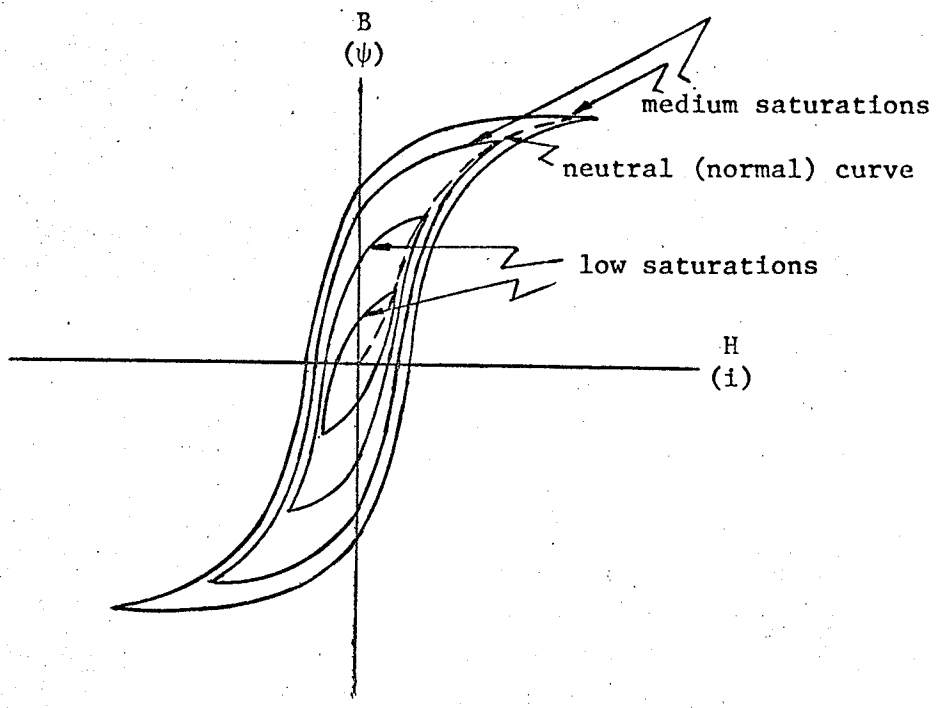

FIGURE 1.4 Hysteresis Curves of Low and Medium Saturations.

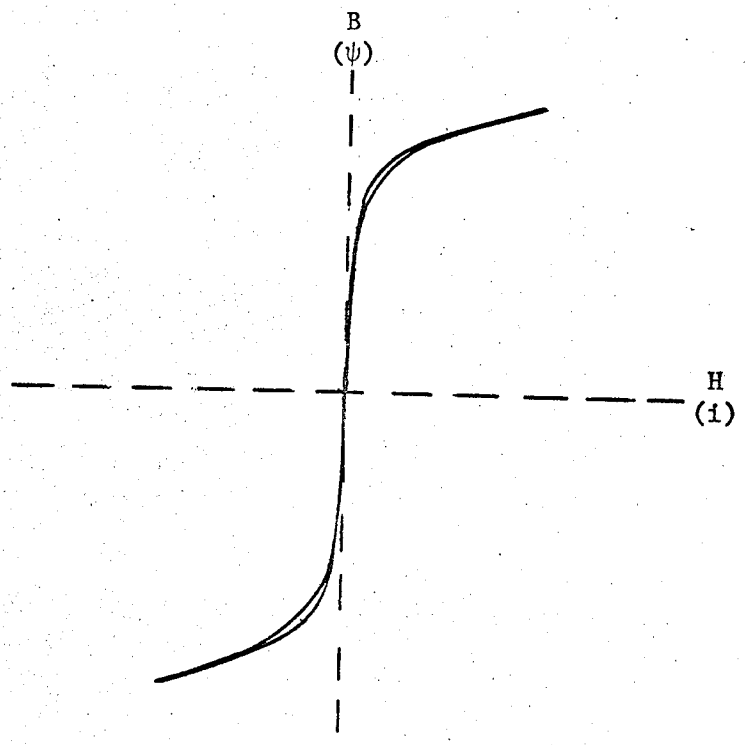

FIGURE 1.5 Hysteresis Curve of High Saturation.

saturations* are shown in Fig. 1.4. The closed hysteresis loop of high saturation is shown in Fig. 1.5.

I.3 Hysteresis.

The area enclosed by the hysteresis loop as shown in Fig. 1.4 represents the amount of energy loss in the form of heat and noise. The larger the area, the higher will be the energy loss. Therefore, it is desirable to design the transformers and reactors to have as low a hysteresis loss as possible; however, a wider hysteresis loop is required for digital computer storage purposes.

The mathematical expression for the hysteresis loss[1]** is:

$$P_h = k \cdot V_o \cdot f \cdot B_m^x \tag{1.11}$$

where P_h is the hysteresis loss

V_o is the volume of the magnetic circuit

f is the applied voltage frequency

B_m is the maximum flux density

k is a hysteresis constant

x is the Steinmetz exponent.

For modern iron commonly used, x is between 1.6 to 2; and k is small, so the hysteresis loss is low.

Finzi[2] has shown that if the iron core is energized with alternating current, only a small amount of hysteresis loss is present. A typical

---

*Magnetic saturations of a family of closed hysteresis loops may be classified into low saturation, medium saturation and high saturation.

** Superscript indicates reference in bibliography.

high-saturation hysteresis loop of a wound-core transformer energized with 60 cycle alternating voltage is shown in Fig. 1.5. A study of the high-saturation hysteresis loop reveals that the hysteresis loop is very narrow. Fortunately, subharmonic oscillations occur only when the core is highly saturated. At high saturation, the hysteresis loss is negligibly small, so it is reasonable to neglect the hysteresis in analysing the subharmonic response.

I.4 The Magnetic Characteristic Curve of a Shunt Reactor.

Theoretically, the most simple form of a reactor is a ring core closely surrounded by the windings. Provided that the ratio of the outer to inner radius of the core is a little greater than 1, a current through the core windings will induce a flux of approximately the same uniformity in the core and only a negligible flux outside the core. The total flux linkages of a reactor is:

$$\psi_T = \psi_c + \psi_\ell \tag{1.12}$$

where ψ_T is the total flux linkages of the reactor

ψ_c is the flux linkages of the core

ψ_ℓ is the flux linkages of the leakage path of the core.

Since ψ_ℓ is negligibly small, equation (1.12) can be written as:

$$\psi_T \simeq \psi_c \tag{1.13}$$

But in practice, due to the influence of the air gaps present in the core

of the reactor used for shunt compensation in transmission lines, the flux linkages of the leakage path ψ_ℓ is considerable in comparison with the flux linkages of the core ψ_c; as a result the reactor does not have such a simple "ideal" form as described above in Equation (1.13).

Figure 1.6 shows the magnetic characteristic curve of a shunt reactor constructed from the ideal core curve, air-gap line and the line of the flux linkages of the leakage path. If we refer to Figure A.1 in Appendix A, page 64, we may use the fact that the flux linkages in the air-gap are caused by a current flowing through the air-gap inductance, L_a. We may then say that at any time, t, the current through L_a is I_a. We may also use a similar approach for the core inductance, L_c; and so at the same instant of time, t, we will have a current, I_c, passing through L_c. The total current, I_T, will then be equal to $I_a + I_c$, and this current flows through the shunt reactor. Hence, any point on the locus of $I_a + I_c$ may be obtained as shown in Figure 1.6. It then remains to determine the ψ_T component in the $i - \psi$ plane. Now at the same instant of time, t, since the total flux linkages, ψ_T are equal to $\psi_c + \psi_\ell$, we may obtain the value of ψ_T as the ordinate of the point, p, on the $I_a + I_c$ locus as shown. If the same procedure is followed for several points, the real magnetic characteristic curve of the shunt reactor may be constructed as shown in the diagram.

In Figure 1.6, the lower portion of the magnetic characteristic curve is called the linear portion of the magnetic characteristic curve. The point, p', where the transistion begins from the linear portion to the non-linear portion is called the "knee" of the magnetic characteristic curve. The upper portion which is above the point p' is termed the

non-linear portion of the magnetic characteristic curve. Obviously, the presence of the air gaps in the core is able to extend the range of the linear portion of the magnetic characteristic curve of the shunt reactor.

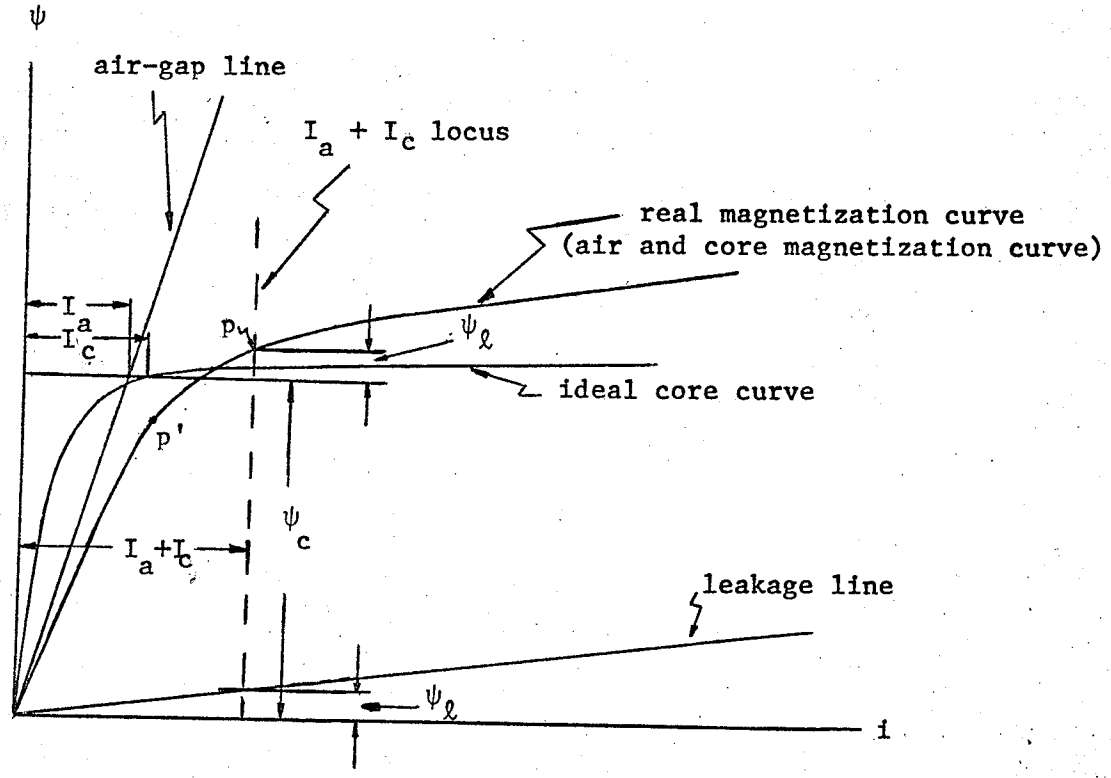

FIGURE 1.6 Construction of a Real Magnetic Characteristic Curve of a Shunt Reactor.

CHAPTER II

ASPECTS OF EXTRA-HIGH-VOLTAGE EXTRA-LONG-DISTANCE TRANSMISSION LINES

There are four basic parameters in a transmission line. Line resistance and line reactance make up the line series impedance. Line susceptance and line conductance determine the shunt admittance. But, the conductance is very small in comparison with the line susceptance at power frequency and thus it can be neglected. If representing a long transmission line by an equivalent π circuit, suitable line correction factors for line resistance, line reactance and line susceptance are required.

The increasingly large demand of electric power focuses attention onto the use of extra-high-voltage for transferring bulk power from the remote power plant to the load centre. Thus, not only are the old problems intensified, but also new problems are created.

II.1 Power Transfer.

An object which attracts the attention of line design engineers is the amount of power which can be transferred to the load center. Fig. 2.1

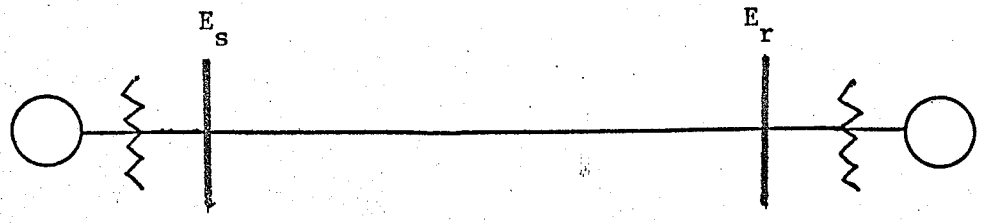

FIGURE 2.1 A Single-line Diagram of a Power Transmission System.

shows a single-line diagram of a power transmission system. Under steady-state conditions, the power transfer equations from sending end to receiving end are[3]:

$$P_r = \frac{|E_s| \cdot |E_r|}{|B|} \cos(\beta-\theta) - \frac{|A||E_r|^2}{|B|} \cos(\beta-\alpha) \qquad (2.1)$$

$$P_s = -\frac{|E_s||E_r|}{|B|} \cos(\beta+\theta) - \frac{|D||E_s|^2}{|B|} \cos(\beta-\gamma) \qquad (2.2)$$

where P_r is the power received by the system,

P_s is the power delivered to the system,

E_s is the sending end line to line voltage in rms value,

E_r is the receiving end line to line voltage in rms value,

θ is the torque angle between the sending end and receiving end voltages,

A, B and D are the generalized line constants of a four terminal network with their respective phase angles α, β, and γ.

In practice, it is accurate enough to estimate the power transfer by assuming line resistance and shunt admittance to be zero. Then the amount of power transferred is equal to the amount of power received. That is:

$$P_s = P_r = P = \frac{E_s E_r}{X_L} \sin\theta \qquad (2.3)$$

where P is the power transferred or received,

X_L is the pure line reactance from sending end to receiving end in the case under study.

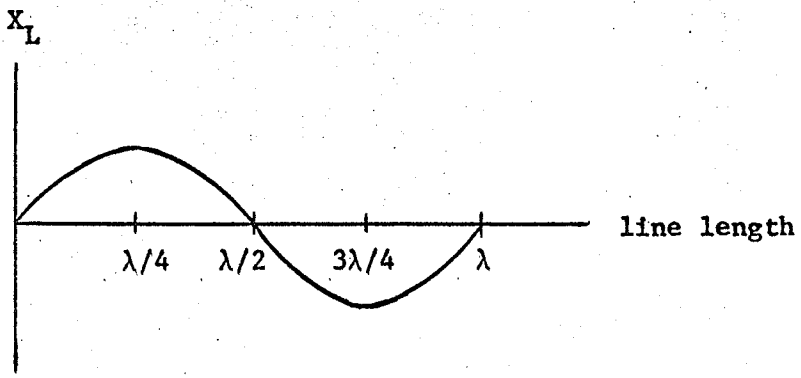

FIGURE 2.2 Line Reactance as a Function of Line Length.

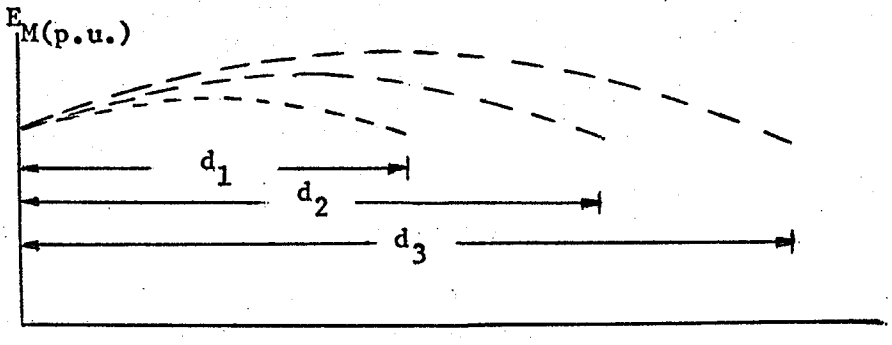

FIGURE 2.3 Mid-point Overvoltage as a Function of Line Length.

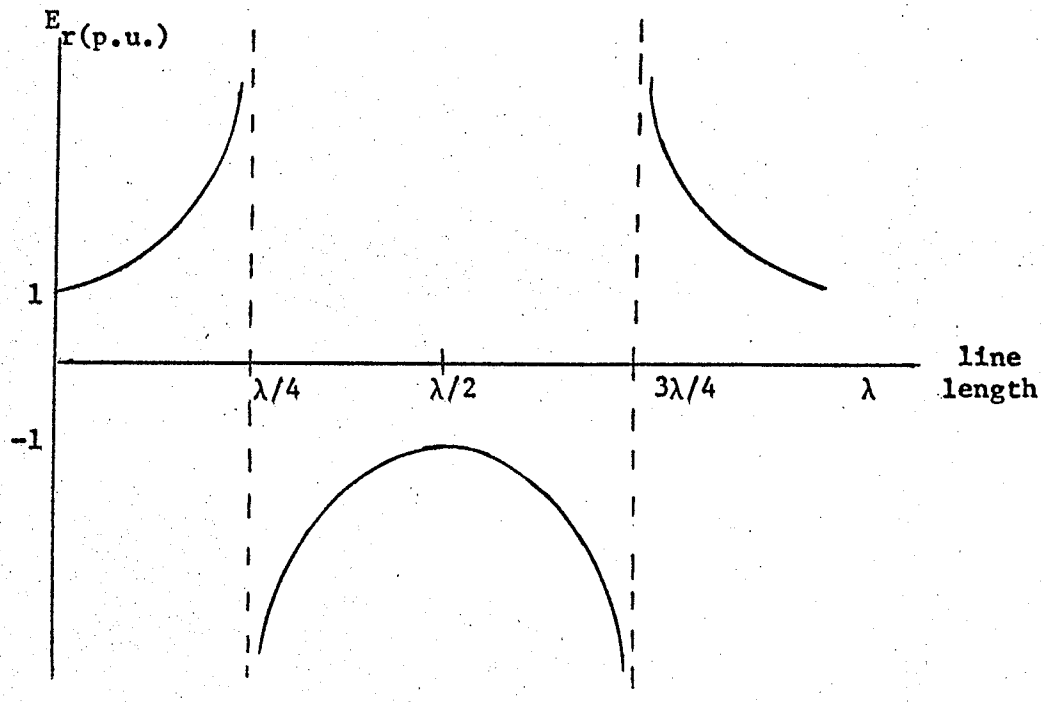

FIGURE 2.4 Receiving End Overvoltage as a Function of Line Length.

Figure 2.2 shows the line reactance, X_L, as a function of line length. The line reactance increases with increasing line length. It approaches the maximum value when the line length reaches a quarter wave length which is approximately equal to 750 miles at 60 Hz frequency. A study of equation (2.3) reveals that the power transfer, P, will be the lowest when the line length is equal to a quarter wave length, if no series compensation is provided.

Figure 2.3* shows the mid-point overvoltage as a function of line length, while the sending end and receiving end voltages are kept constant. The severity of the overvoltage at the mid-point of a transmission line increases with the increase of the line length if no shunt compensation is provided.

Figure 2.4* indicates the open-circuit overvoltage at the receiving end as a function of line length after load rejection. The receiving end overvoltage theoretically approaches infinity for a lossless transmission line at a quarter wave length.

II.2 Transmission Line Sectionalization.

Sectionalization is an artificial means of breaking a very long transmission line into several short lines. Each line section is terminated with a switching station as shown in Fig. 2.5. Obviously, sectionalization not only can increase the reliability of the transmission system, but also can increase its stability limits.

---

*The overvoltages at the mid-point and receiving end shown are expressed in per unit quantities in terms of sending end voltage.

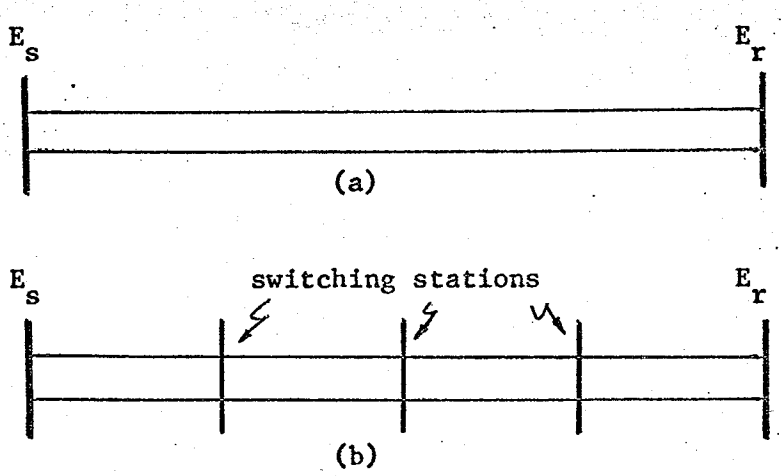

FIGURE 2.5 Sectionalization of ELD Transmission Lines.
(a) Before sectionalization.
(b) After sectionalization.

II.3 Series and Shunt Compensations.

A study of equation (2.3) indicates that the line reactance, X_L, must be reduced in order to increase the power transfer. The use of a bundle conductor to reduce X_L is not too effective, and the increase of the number of circuit lines is not economical. The most effective and economical method which attracts the attention of the line design engineers is the use of series capacitors. To reduce the mid-point overvoltage and the serious overvoltages caused by faults or load rejection, shunt compensation is required. Figure 2.6 shows an equivalent circuit of a section of a transmission line compensated with series capacitors and shunt reactors.

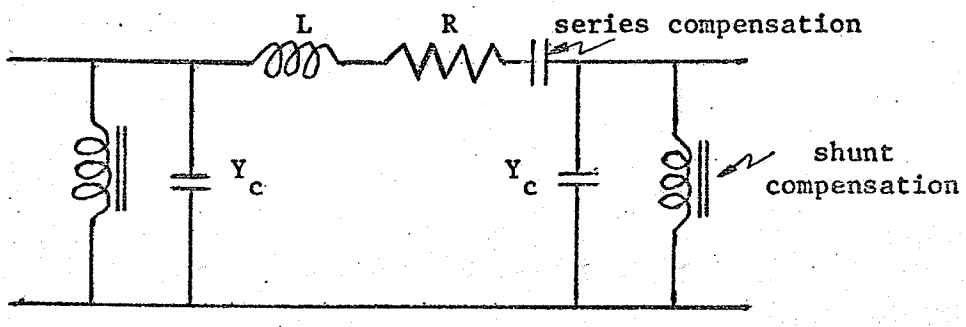

FIGURE 2.6 An Equivalent Circuit of a Line Section.

II.4 Overvoltages Caused by Switching, Load Rejection and Single-Line-to-Ground Fault at No Load.

Though the transmission line may be properly compensated, the overvoltages caused by switching transients, load rejection and single-line-to-ground fault at no load are still of special interest. These overvoltages may "shock" the system to give rise to sustained subharmonic oscillations. (See Chapter III).

II.4.1 Switching transients:

In energizing an extra-high-voltage extra-long-distance (EHV ELD) transmission line, circuit breakers are closed. Hence, the switching transients shown in Figure 2.7 are introduced. Due to the influence of the magnetic characteristic of the shunt reactor, both the amplitude and frequency of the service voltage are affected. Fortunately, the transient overvoltages die out as time goes on.

II.4.2 Overvoltages caused by load rejection and single-line-to-ground fault at no load.

The overvoltage caused by load rejection or open circuit at the receiving end will not be as severe as in Figure 2.4 if the line is compensated; but it is still quite considerable. At no load with single-line-to-ground fault, overvoltages will result on the two healthy phases. Due to the presence of the positive, negative and zero sequence impedances, the overvoltages on the two healthy phases will not be equal. The overvoltages resulting from load rejection and single-line-to-ground fault at no load are shown in Figure 2.8.

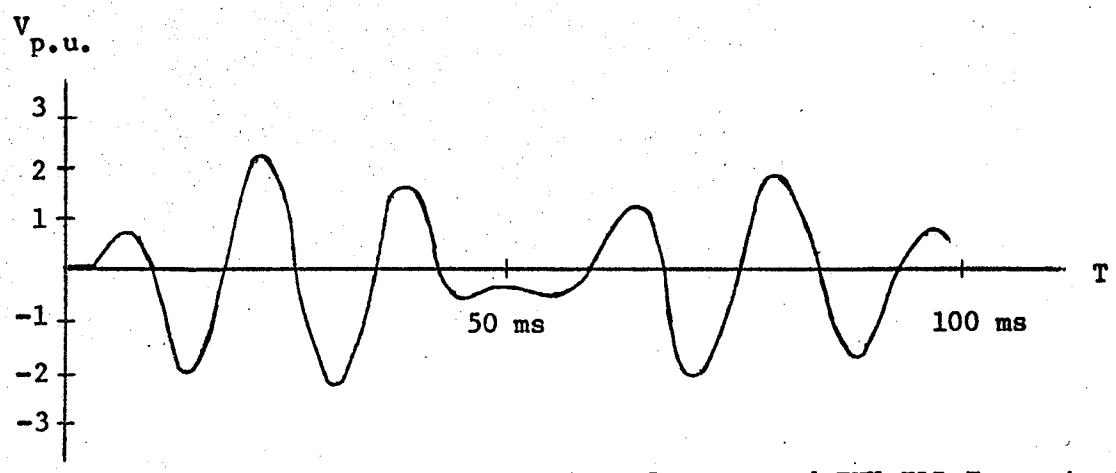

FIGURE 2.7 Switching Transients in a Compensated EHV ELD Transmission Line.

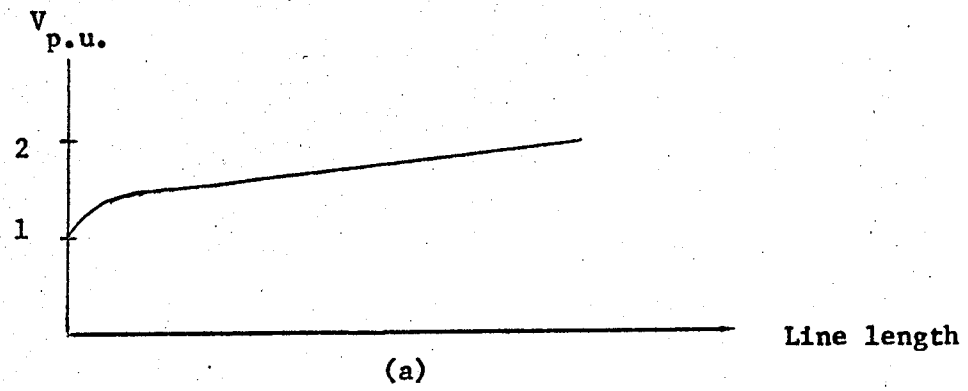

(a)

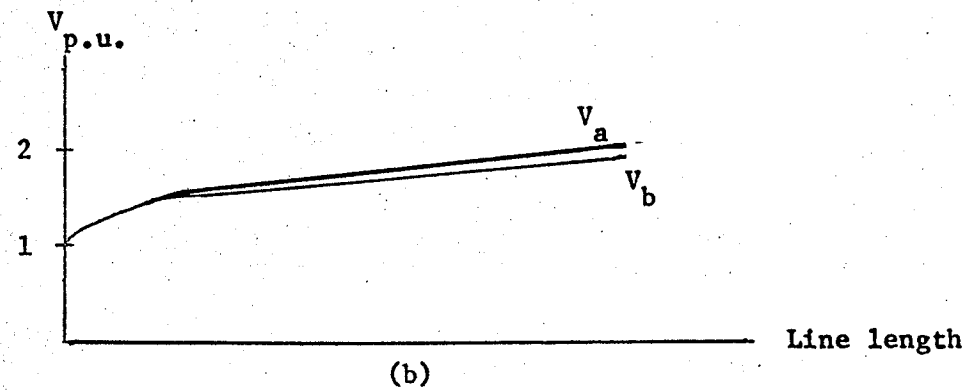

(b)

FIGURE 2.8 Overvoltages as a Function of Line Length.

(a) Load rejection
(b) Single-line-to-ground fault at no load.

CHAPTER III

ANALYSIS OF SUBHARMONIC OSCILLATIONS

Under a relatively limited condition, the applied sinusoidal voltage to a non-linear system gives rise to sustained subharmonic oscillations. The response of subharmonic oscillations is a high-magnitude, low-frequency type oscillation, whose frequency is a fraction (i.e. $\frac{1}{n}$, where $n = 2, 3, 4, \ldots$) of the applied voltage frequency. The subharmonic is of the order n, i.e., when the applied voltage completes one cycle the subharmonic completes $\frac{1}{n}$ cycle. The presence of abnormally high current and high voltage resulting from the subharmonic response, not only causes interference to the system, but also endangers the life of the series capacitors.

III.1 Subharmonic Occurrence.

The use of shunt reactors in conjunction with capacitors in a transmission line results in a non-linear circuit. Under suitable conditions, subharmonic oscillations will occur only if a "shock" or a "transient" is introduced.

The equivalent circuit representing the transmission line with series and shunt compensations is shown in Figure 3.1. The line resistance and line inductance are retained to represent the actual system. Most of the previous authors[4,5,6] included the line inductance with that of the shunt reactor. Glavitsch[7] even neglected both the line inductance and the

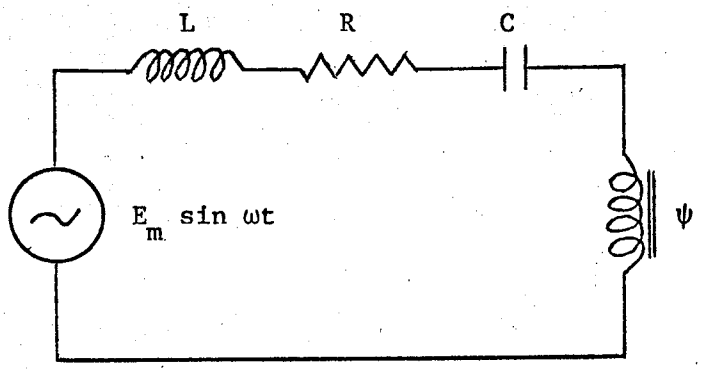

FIGURE 3.1 Modified Circuit of an EHV ELD Transmission Line.

R = Line resistance L = line inductance
C = Series capacitance ψ = Flux linkages of the shunt reactor.

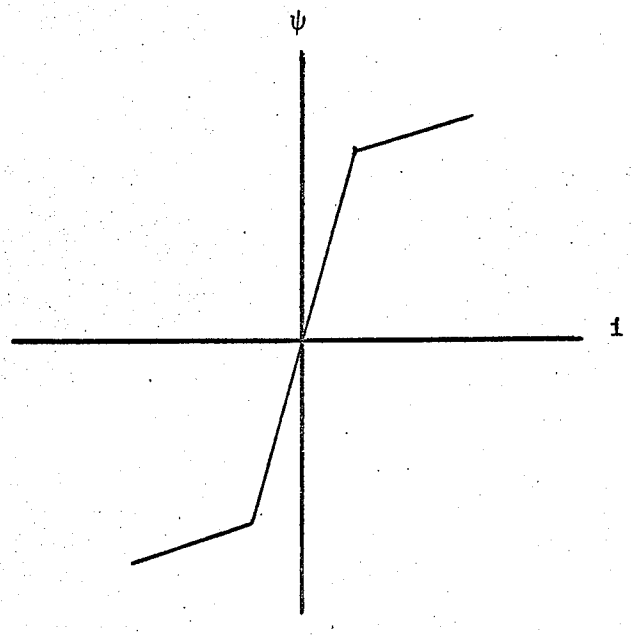

FIGURE 3.2 i - ψ Relationship.

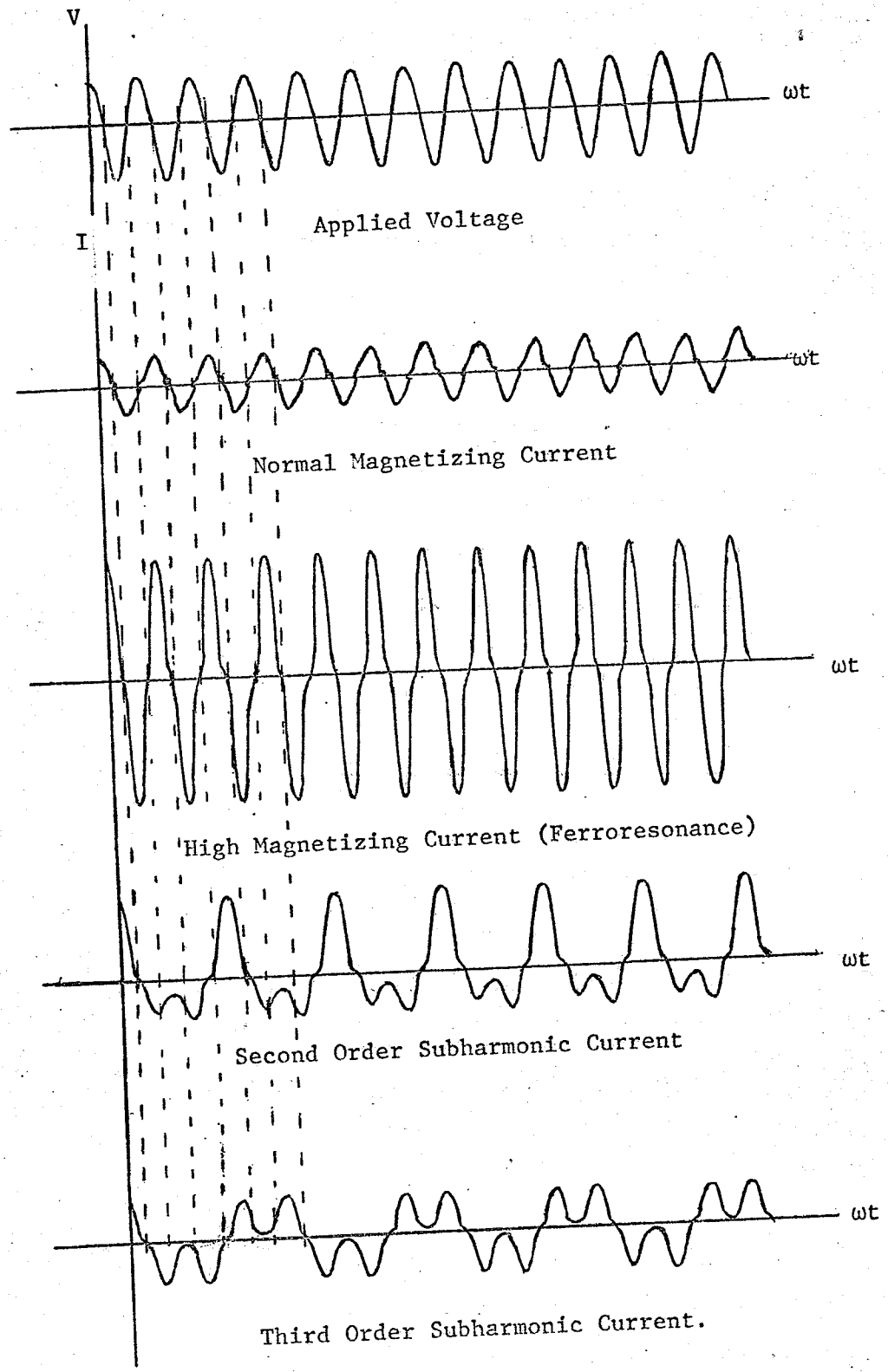

FIGURE 3.3 Typical Voltage and Current Waveforms
(not drawn to scale and phase relationship not maintained)

line resistance in the analysis of the subharmonic oscillations. The linearized magnetic characteristic curve of the shunt reactor used in this study is shown in Figure 3.2, where hysteresis is neglected. The inductance of the reactor is very high before saturation, and is very low after saturation.*

As mentioned previously, subharmonic oscillations only occur under limited conditions. If these oscillations do not exist after the "shock" the system will operate at the service voltage frequency either in the "normal magnetizing current" state or the "high magnetizing current" state. Typical voltage and current waveforms are shown in Figure 3.3.

III.2. Stability of Subharmonic Oscillations.

Subharmonics can be classified into stable subharmonics and unstable subharmonics. Literally, any type of subharmonic which has constant magnitude and definite order is termed a stable subharmonic. An unstable subharmonic does not have any definite order and may disappear suddenly after its occurrence.

In a non-linear control system, a subharmonic response circuit may be represented by a single-loop feedback system[8, 9] as shown in Figure 3.4. The non-linear element representing the shunt reactor has a gain N which depends only on the amplitude of the input signal e_i to the non-linear element. The linear element representing the combination of R, L and c of Figure 3.1 has a gain G which depends only on the frequency to the linear element. The closed-loop gain of the system is:

$$K_c = \frac{\text{Input}}{\text{Output}} = \frac{N.G}{1 + N.G} \qquad (3.1)$$

---

* See Appendix A.(a).

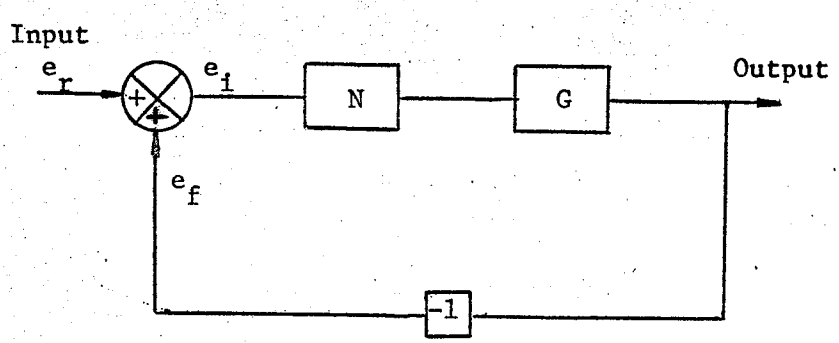

FIGURE 3.4 Block Diagram of a Subharmonic System

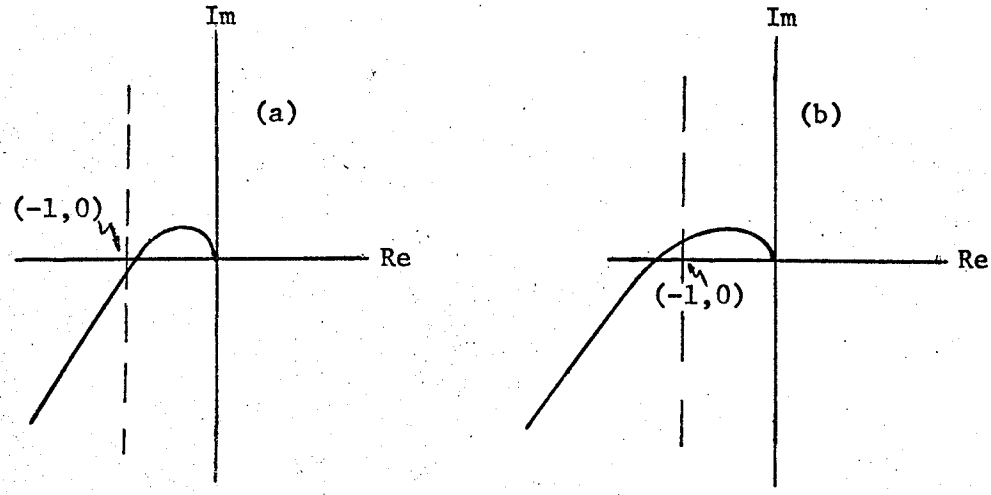

FIGURE 3.5 Locus of G. (a) Stable Oscillation, (b) Unstable Oscillation.

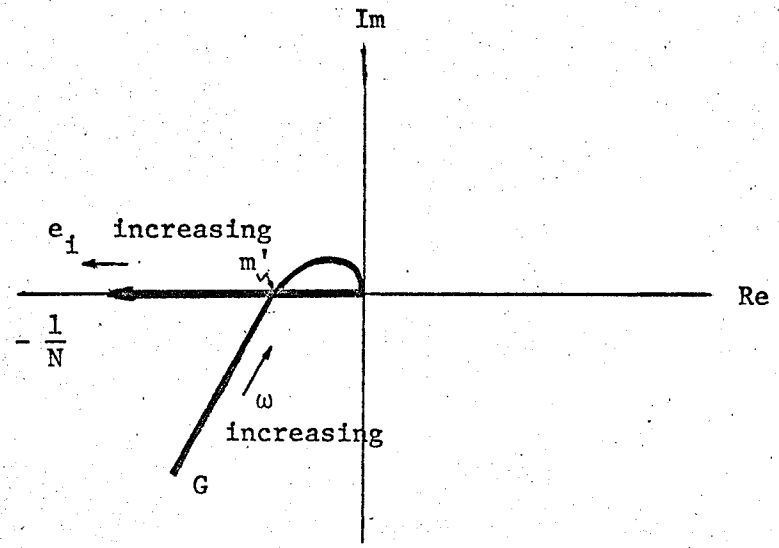

FIGURE 3.6 A Conventional Describing Function Diagram

and the open-loop gain is:

$$K_o = \frac{\text{Output}}{\text{Input}} = N.G \tag{3.2}$$

The condition for stable subharmonic oscillations is such that the G, locus of the linear portion of the open-loop gain plotted on the complex plane, must not enclose the $(-1,0)$ point as shown in Figure 3.5. It implies that the open-loop gain K_o must be -1. That is:

$$N.G = -1 \tag{3.3}$$

or

$$G = -\frac{1}{N} \tag{3.4}$$

Equation (3.4) is known as describing function. Plotting G and $-\frac{1}{N}$ on the complex plane, the point of intersection of the two loci gives the required amplitude and frequency for stable subharmonic oscillations. However, since the describing function depends on the four parameters: a, b, $\frac{1}{n}\omega$ and ϕ of the input signal e_i,* the solution for a

---

*The input signal e_i, to the non-linear element is a combination of the reference input $(e_r = a \sin \omega t)$ and the feedback $(e_f = b \sin(\frac{1}{n}\omega t + \phi))$:

$$e_i = a \sin \omega t + b \sin\left(\frac{1}{n}\omega t + \phi\right)$$

where a is the amplitude of the reference input e_r
b is the amplitude of the feedback e_f
$\frac{1}{n}\omega$ is the subharmonic frequency
ϕ is the phase relationship between the reference input and the feedback.

stable subharmonic response will be very complicated and is not so simple as described above.

A conventional describing function illustrating the characteristics of the two loci and their intersection point, m', is shown in Figure 3.6.

III.3 The Effects of Circuit Parameters.

III.3.1 Line resistance.

Knudsen[4] expressed the relative loss factor for a R-L(i)-C series circuit with non-linear inductance L(i) to determine the subharmonic response as:

$$\delta = R\omega C = \frac{R}{X_c} \tag{3.5}$$

where δ is the relative loss factor

R is the resistance

C is the series capacitance

ω is the service voltage frequency.

The relative loss factor of Equation (3.5) varies with the increase or decrease of R if C is kept constant.

A study of Figure 3.7 reveals that the magnitude of subharmonic current increases with decrease of the relative loss factor. In order to maintain the subharmonic oscillations, the applied voltage must be of a magnitude enough to overcome the energy dissipated by the resistance. If the value of the relative loss factor is higher than the critical value δ_c, no subharmonic can occur even though the applied voltage can compensate the resistance voltage drop.

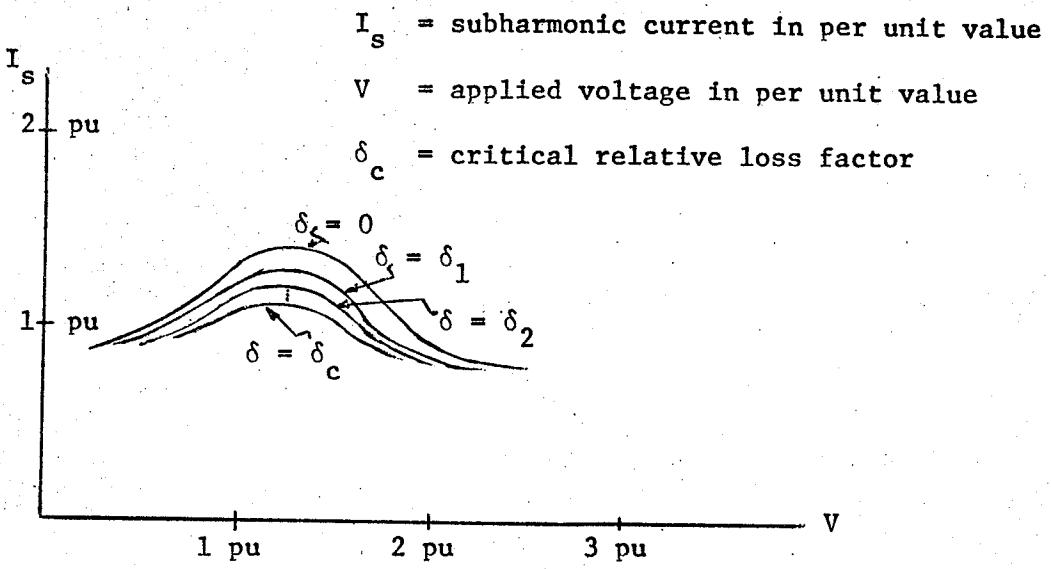

FIGURE 3.7 Characteristic Curves of the Relative Loss Factor with Constant X_c.

III.3.2 Series capacitance.

Refer to Equation (3.5); the relative loss factor is:

$$\delta = \frac{R}{X_c} \tag{3.5}$$

Keeping the line resistance, R, constant, and varying the capacitance, the subharmonic response curves will not be the same as shown above, i.e., Figure 3.7. Instead, the subharmonic response curves are inverse as shown in Figure 3.8*.

---

*McCrumm[10] stated, "If the capacitance be reduced but resistance left unchanged, then for a given voltage, the subharmonic current will be less", and "increasing the capacitance produces much the same effect except that the resulting current is larger."

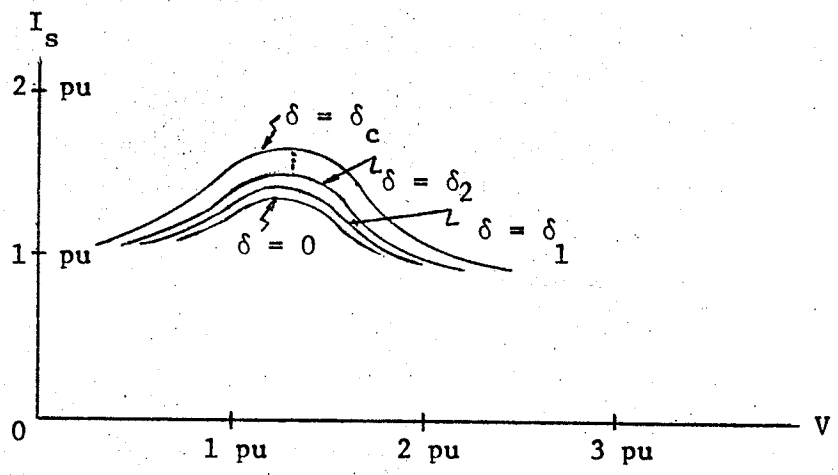

FIGURE 3.8 Characteristic Curves of the Relative Loss Factor with Constant R.

In order to visualize the relationship between the capacitance and the resistance, attention is centered on the capacitance-resistance curves shown in Figure 3.9.[10] Outside the boundary of the curve 1, no subharmonic will occur. The area between curve 1 and curve 2 gives the stable subharmonic oscillations. Unstable subharmonics can exist in the region below curve 2. The dotted lines of the two curves indicate that a further decrease of resistance or increase of capacitance may result in unstable subharmonics. Figure 3.9 also shows that there is a critical value for capacitance below or beyond which no subharmonic can exist.

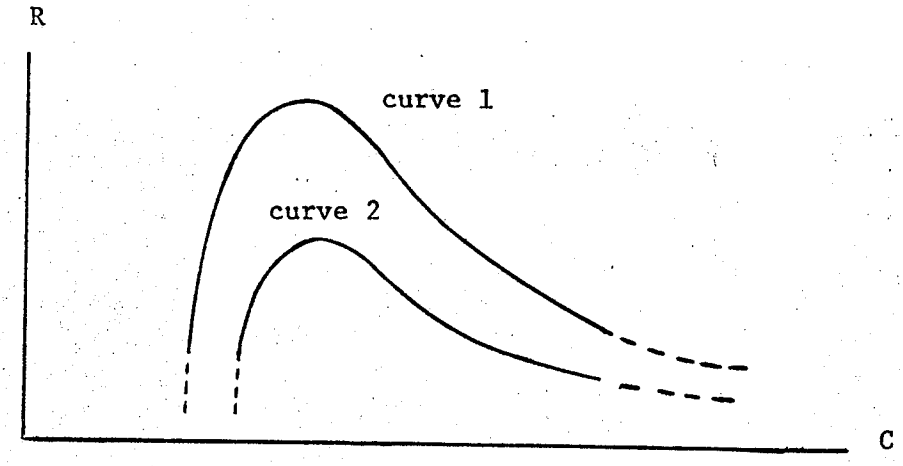

FIGURE 3.9 Limiting Region for Stable Subharmonic Oscillations.

III.3.3. Shunt reactor.

The linear range of the magnetic characteristic of a shunt reactor is one of the important factors in determining the occurrence of subharmonic oscillations. No subharmonic will occur if a shunt reactor remains unsaturated. To saturate the shunt reactor, the applied voltage must reach the knee of the magnetic characteristic of the reactor. If the magnitude of the voltage is sufficiently high, the reactor can be saturated every half cycle.

Portnoi[6] has shown that the subharmonic response is determined by the inductance of the linear portion of the shunt reactor and the series compensation level. Hence, the subharmonic frequency is:

$$f_s = \frac{1}{2\pi\sqrt{L_{lin}\,C}} \qquad (4.6)$$

where f_s is the subharmonic frequency

C is the series capacitance

L_{lin} is the inductance of the linear portion of the magnetic characteristic of the shunt reactor.

In varying the linear range of the shunt reactor, the subharmonic response will change. If the shunt reactor is so designed that its linear range is far above the applied voltage, subharmonics will not occur. Such a linear range is probably best determined by means of experiment.

III.4 The Effect of Applied Voltage.

The applied voltage is an essential source to overcome the energy dissipated by the resistance. If the applied voltage increases gradually from zero, the current will only follow the magnetic characteristic curve

of the shunt reactor. As stated previously, subharmonic oscillations will occur only if a "shock" is introduced. These oscillations will cease if the applied voltage cannot compensate for the energy dissipated by the resistance. However, for the given circuit parameters, there is an upper and lower limit for the applied voltage below or beyond which no subharmonic response is possible. The current will either oscillate at a low current state known as "normal magnetizing current" or a high current state known as "ferro-resonance". The phenomenon of ferroresonance is a very high current oscillation which oscillates at the applied voltage frequency. This phenomenon is more severe than the phenomenon of subharmonic oscillation. It should be avoided at all costs. (See Figure 3.3, page 22).

III.5 The Effects of Initial Conditions.

It has been recognized that the initial conditions are the governing factors which determine the possibility of the initiation of subharmonic response in a non-linear circuit. These initial conditions are:

(a) Point of the applied voltage wave (switching angle),

(b) Initial charge on the capacitor,

(c) Initial flux linkages of the reactor.

A high transient inrush current will saturate the shunt reactor if the applied voltage is closed at zero point of the applied voltage wave or other effective points[5, 11] (i.e. 30°, 45°, 60° ...). The high transient inrush current can only last for a few cycles if the circuit is without an energy storage element (capacitor). But in an EHV ELD transmission line, series compensation is at a high level, so the inrush current will persist to saturate the reactor. Due to the magnetic characteristic of the shunt

reactor and the attentuation of the line resistance, the magnitude of the inrush current reduces as the frequency decreases. The reduction of the magnitude of the inrush current will cease when its frequency becomes a fraction of the applied voltage frequency. Then the inrush current is transformed into subharmonic current[6]. These oscillations will be maintained by the energy derived from the source. The typical reductions of magnitude and frequency are shown in Figure 3.10.

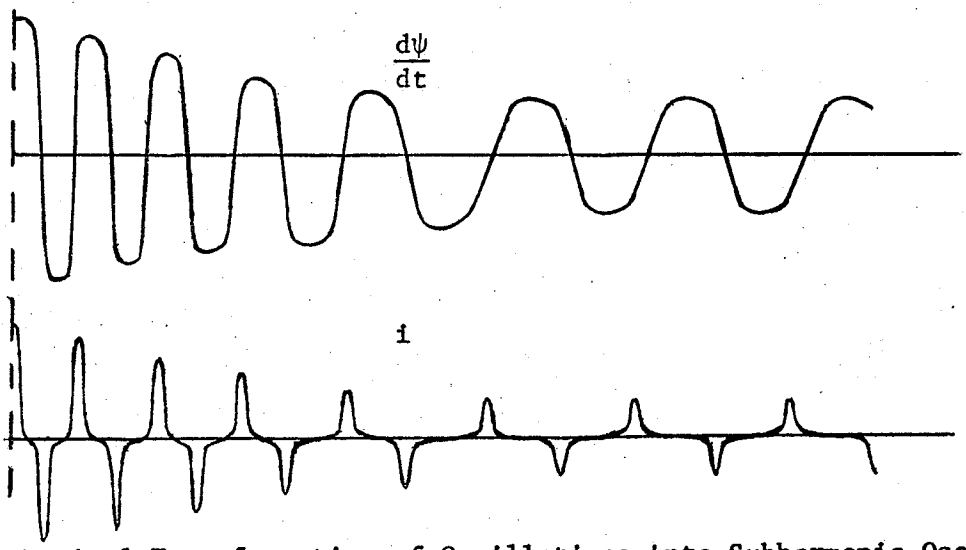

FIGURE 3.10 Typical Transformation of Oscillations into Subharmonic Oscillations.

A similar effect will result if either the initial charge on the capacitor or the initial flux linkages of the shunt reactor is sufficient to saturate the reactor.

CHAPTER IV

MATHEMATICAL ANALYSIS

In attempting a mathematical analysis of a non-linear series circuit, most of the previous authors approximated the magnetic charactersitic curve of the shunt reactor or the transformer by a mathematical series. These series are:

(a) Power series, like

$$i = a_o + a_1\psi + a_2\psi^2 + \ldots + a_\kappa\psi^\kappa$$

(b) Fourier series, like

$$i = \frac{a_o}{2} + \sum_{\kappa=1}^{\infty} (a_\kappa \cos \kappa\psi + b_\kappa \sin \kappa\psi)$$

where a_o, a_1, b_1, a_2, b_2, .., and a_κ, b_κ are constants. Obviously, considerable difficulty is encountered when any one of the above series is substituted into the differential equation or equations of the non-linear circuit and the general solution attempted. However, the problem can be circumvented by the use of three straight lines to approximate the magnetic characteristic curve. These three straight lines divide the characteristic curve into three regions with two saturation points, P_1 and P_2 as shown in Figure 4.1(b). The solution is discussed below:

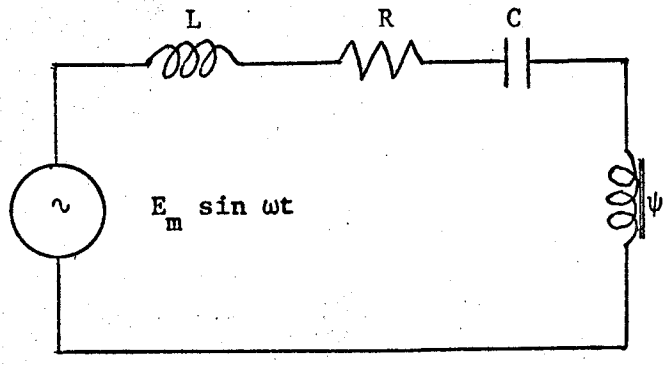

FIGURE 4.1(a) Modified EHV ELD Transmission Circuit

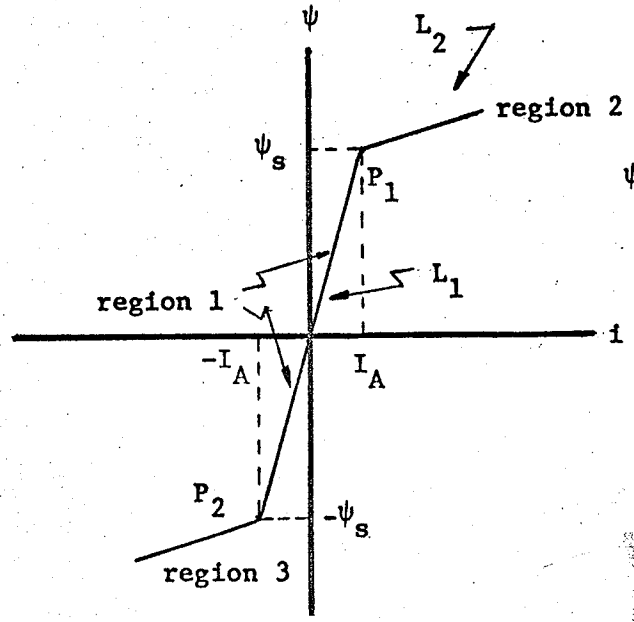

ψ_s = saturation point (linear range) of the shunt reactor.

FIGURE 4.1(b) i - ψ Nonlinearity.

IV.1 Solution of Region 1.

The equivalent circuit for studying the subharmonic response shown in Figure 3.1(a) is redrawn in Figure 4.1(a), and the non-linearity representing the characteristic of the shunt reactor shown in Figure 3.1(b) is redrawn in Figure 4.1(b). The differential equation for Figure 4.1(a) is:

$$L\frac{di}{dt} + Ri + \frac{1}{C}\int i dt + \frac{d\psi}{dt} = E_m \sin \omega t \qquad (4.1)$$

When the shunt reactor operates in the unsaturated region, that is in Region 1, the current and the magnetic flux linkages are:

$$i < |I_A| \qquad \text{and} \qquad \psi = L_1 i^* \qquad (4.2)$$

Substituting Equation (4.2) into Equation (4.1) yields:

$$(L + L_1)\frac{di}{dt} + Ri + \frac{1}{C}\int i\, dt = E_m \sin \omega t \qquad (4.3)$$

Let $\omega t = T$, and $\omega dt = dT$, therefore Equation (4.3) becomes:

$$(X_1 + X_L)\frac{di}{dT} + Ri + X_c \int i dT = E_m \sin T \qquad (4.4)$$

where $X_1 = \omega L_1$, $X_L = \omega L$ and $X_c = \frac{1}{\omega C}$.

---

*See Appendix A, page 63

Differentiating Equation (4.4) with respect to T, we obtain:

$$(X_1 + X_L)\frac{d^2i}{dT^2} + R\frac{di}{dT} + X_c i = E_m \cos T \qquad (4.5)$$

The complete solution of Equation (4.5) is decomposed into two parts. That is:

Complete solution = Complementary function + Particular integral.

IV.1.1 Complementary function i_c.

The homogeneous equation of Equation (4.5) is:

$$(X_1 + X_L)\frac{di^2}{dT^2} + R\frac{di}{dT} + X_c i = 0 \qquad (4.6)$$

where the characteristic equation is:

$$(X_1 + X_L)m^2 + Rm + X_c i = 0 \qquad (4.7)$$

Hence, the roots of Equation (4.7) are:

$$m^2 = -\frac{R}{2(X_1 + X_L)} \pm \sqrt{\frac{R^2}{4(X_1 + X_L)^2} - \frac{X_c}{X_1 + X_L}}.$$

In practice, the line resistance, R, is very small in comparison with the line reactance X_L, and the reactance X_1. Then:

$$(X_1 + X_L)^2 >> R^2.$$

So the roots become:

$$m^2 = -\frac{R}{2(X_1 + X_L)} \pm j\sqrt{\frac{X_c}{X_1 + X_L}}$$

Therefore the solution (complementary function) of Equation (4.6) is:

$$i_c = e^{-\frac{R}{2(X_1 + X_L)}} \left(A_1 \cos \sqrt{\frac{X_c}{X_1 + X_L}}\, T + B_1 \sin \sqrt{\frac{X_c}{X_1 + X_L}}\, T\right) \tag{4.8}$$

where A_1 and B_1 are constants.

IV.1.2 Particular integral i_p.

The choice of particular integral for Equation (4.5) is:

$$i_p = C_1 \cos T + C_2 \sin T \tag{4.9}$$

where C_1 and C_2 are constants.

Differentiating Equation (4.9) once and twice with respect to T, we obtain:

$$\frac{di_p}{dT} = -C_1 \sin T + C_2 \cos T \tag{4.10}$$

$$\frac{d^2 i_p}{dT^2} = -C_1 \cos T - C_2 \sin T \tag{4.11}$$

Substituting Equations (4.9),(4.10), and (4.11) into Equation (4.5) and equating the coefficients of sin T and cos T separately, yields:

$$-C_1(X_1 + X_L - X_c) + C_2R = E_m \tag{4.12}$$

$$-C_2(X_1 + X_L - X_c) - C_1R = 0 \tag{4.13}$$

Solving Equations (4.12) and (4.13) simultaneously, results in:

$$C_1 = -\frac{E_m(X_1 + X_L - X_c)}{R^2 + (X_1 + X_L - X_c)^2}$$

$$C_2 = \frac{E_mR}{R^2 + (X_1 + X_L - X_c)^2}$$

Substituting the values of C_1 and C_2 into Equation (4.9) yields:

$$i_p = -\frac{E_m(X_1 + X_L - X_c)}{R^2 + (X_1 + X_L + X_c)^2} \cos T + \frac{E_mR}{R^2 + (X_1 + X_L - X_c)^2} \sin T \tag{4.14}$$

Setting $\sin T_1 = \frac{X_1 + X_L - X_c}{\sqrt{R^2 + (X_1 + X_1 - X_c)^2}}$ and $\cos T_1 = \frac{R}{\sqrt{R^2 + (X_1 + X_L - X_c)^2}}$,

and substituting $\sin T_1$ and $\cos T_1$ into Equation (4.14) yeilds:

$$i_p = \frac{E_m}{\sqrt{R^2 + (X_1 + X_L - X_c)^2}} (-\cos T \sin T_1 + \sin T \cos T_1) \tag{4.15}$$

Rearranging Equation (4.15) yields the particular integral:

$$i_p = \frac{E_m}{\sqrt{R^2 + (X_1 + X_L - X_c)^2}} \sin (T - T_1) \tag{4.16}$$

Combining Equations (4.8) and (4.16), gives the complete solution of Equation (4.5) in Region 1. That is:

$$i_1 = \frac{E_m}{\sqrt{R^2 + (X_1 + X_L - X_c)^2}} \sin (T - T_1) + e^{-\frac{R}{2(X_1 + X_L)} T} \left[A_1 \cos \sqrt{\frac{X_c}{X_1 + X_L}}\, T + B_1 \sin \sqrt{\frac{X_c}{X_1 + X_L}}\, T\right] \qquad (4.17)$$

IV.2 Solutions of Region 2 and Region 3.

When the shunt reactor operates in the saturated region, that is either in Region 2 or Region 3, the current and the magnetic flux linkages are:

$$i > |I_A| \quad \text{and} \quad \psi = L_2 i^* \qquad (4.18)$$

Substituting Equation (4.18) into Equation (4.1) yields:

$$(L + L_2) \frac{di}{dt} + Ri + \frac{1}{C}\int idt = E_m \sin \omega t \qquad (4.19)$$

Let $\omega t = T$ and $\omega dt = dT$, therefore Equation (4.19) becomes:

$$(X_2 + X_L) \frac{di}{dT} + Ri + X_c \int idT = E_m \sin T \qquad (4.20)$$

where $X_2 = \omega L_2$

---

*See Appendix A, page 63

Differentiating Equation (4.20) with respect to T, then gives:

$$(X_2 + X_L)\frac{d^2i}{dT^2} + R\frac{di}{dT} + X_c i = E_m \cos T \qquad (4.21)$$

The procedure of solving Equation (4.21) to obtain the complete solution is the same as solving Equation (4.5). Therefore, the complementary function is:

$$i_c = e^{-\frac{R}{2(X_2 + X_L)}T}\left[A_2 \cos\sqrt{\frac{X_c}{X_2 + X_L}}\,T + B_2 \sin\sqrt{\frac{X_c}{X_2 + X_L}}\,T\right] \qquad (4.22)$$

where A_2 and B_2 are constants.

and the particular integral is:

$$i_p = \frac{E_m}{\sqrt{R^2 + (X_2 + X_L - X_c)^2}}(-\cos T \sin T_2 + \sin T \cos T_2) \qquad (4.23)$$

where $\sin T_2 = \frac{E_m}{\sqrt{R^2 + (X_2 + X_L - X_c)^2}}$ and $\cos T_2 = \frac{R}{\sqrt{R^2 + (X_2 + X_L - X_c)^2}}$

Rearranging Equation (4.23) yields:

$$i_p = \frac{E_m}{\sqrt{R^2 + (X_2 + X_L - X_c)^2}} \sin (T - T_2) \qquad (4.24)$$

Combining Equations (4.22) and (4.24), gives the complete solution i_2 of Equation (4.5) in Region 2 and Region 3. That is:

$$i_2 = \frac{E_m}{\sqrt{R^2 + (X_2 + X_L - X_c)^2}} \sin (T - T_2) + e^{-\frac{R}{2(X_2 + X_L)} T} \cdot \left[A_2 \cos \sqrt{\frac{X_c}{X_2 + X_L}}\, T + B_2 \sin \sqrt{\frac{X_c}{X_2 + X_L}}\, T\right] \qquad (4.25)$$

IV.3 Summary.

The two sets of arbritrary constants A_1, B_1 and A_2, B_2 in Equations (4.17) and (4.25) are determined by the boundary conditions (i.e. initial current, initial charge on the capacitor and initial flux linkages of the reactor). Once A_1, B_1 and A_2, B_2 are known, using the step-by-step method, the subharmonic current waveforms can be drawn from Equations (4.17) and (4.25). When the subharmonic current oscillates in Region 1, Equation (4.17) is used to plot the current waveforms. Equation (4.25) is used when the subharmonic current oscillates in Region 2 or Region 3. If the subharmonic current is in the transition points, either equation is valid.

It should be noted that, when the subharmonic current oscillates from Region 1 to Region 2 and back again, and then enters into the negative Regions 1 and 3 and back again, to complete the positive and negative subharmonic current waveforms, this will give rise to very strong transient oscillations.[12, 13] These transient oscillations will restart at each transition from region to region; and thus will continue to oscillate

indefinitely if once initiated, even though a resistive element is considered as in the equivalent circuit of Figure 4.1(a).

The capacitor voltage equations, in the unsaturated and saturated regions, can be obtained by integrating the subharmonic current Equations (4.17) and (4.25) respectively. Using the same procedure as that for drawing the subharmonic current waveforms the capacitor voltage waveforms can be obtained.

It must be remembered that the use of a step-by-step method to draw the subharmonic oscillation waveforms is very laborious. An alternative method is the use of a X-Y recorder connected to the amplifier outputs of an analogue computer to draw the required subharmonic waveforms. The analogue computer method is discussed in CHAPTER V.

CHAPTER VI

CONCLUSIONS

The use of three straight lines to approximate the magnetic characteristic curve of a shunt reactor is more convenient than the use of a mathematical series approximation in the mathematical analysis of subharmonic response. The power series used by Knudsen[4] and the Fourier series used by Hayashi[15] to approximate the magnetic characteristic curve i.e. $i = \psi^3$ and $i = i_o + K_1 \sin \psi + K_2 \cos \psi + K_3 \cos K\psi$ respectively, are not very practical, because the subharmonic response is accompanied by very high saturation of the shunt reactor. The low order of either the power series or the Fourier series used to express the magnetic characteristic of a very high saturation reactor is not suitable, though the solution of a lower power order differential equation is more conveniently obtained.

It is feasible to use an analogue computer (mathematical model) to predict the subharmonic response. Alden[14] has shown that the results obtained from the analogue computer are coincident with the actual tests. However, the operation of an analogue computer is time-consuming. Hence, the use of a digital computer to predict subharmonic response is recommended if the operation cost is reasonable.

In an extra-high-voltage extra-long-distance transmission line, the third order subharmonic will occur at a high series compensation level if the conditions are "favourable" and a "shock" is introduced. With a further increase of the series compensation to a very high level, a second order

Line Data*

	per mile	600 miles†
Reactance per phase X_L	0.51 ohm	235 ohm
Resistance " " R	0.0298 ohm	10.13 ohm
Susceptance " " Y_c	8.08×10^{-6} ℧	5.56×10^{-3} ℧

For a 500 KV service voltage, the natural load is 997 MW per line circuit.

Series Compensation Data

Series compensation levels (percentage of X_L)	ohmic values	per unit values††
0%	0	0
10%	23.5	.0935
20%	47.0	.187
30%	70.5	.281
40%	94.0	.375
50%	117.5	.468
60%	141.0	.562
70%	164.5	.655
80%	188.0	.748
90%	211.0	.844
100%	235.0	.936

Usually, the linear range of the magnetic characteristic of a shunt reactor for an EHV ELD transmission line is 1.2 per unit, which is 0.2 per unit above the service voltage.

*See Appendix B.

†Line corrections are required for equivalent π circuit of an ELD line. A 600 miles long transmission line with line corrections is 461 miles, 340 miles and 688 miles for reactance, resistance and susceptance, respectively.

†† i) See Appendix C.
ii) The bases are:
Base voltage: 500 KV rms or $500\sqrt{2}$KV peak value
Base MVA : 997 MVA.

V.2 The Analogue Computer Circuit.

The differential equation of the modified transmission line circuit of Figure 4.1(a), page 33 is:

$$L\frac{di}{dt} + Ri + \frac{1}{C}\int idt + \frac{d\psi}{dt} = E_m \sin \omega t \qquad (4.1)$$

Expressing Equation (4.1) in per unit quantitites* yields:

$$L_p\frac{dI_p}{dT_p} + R_pI_p + \frac{1}{C_p}\int I_p\, dT_p + \frac{d\psi_p}{dT_p} = \sin T_p \qquad (5.1)$$

or

$$X_{L_p}\frac{dI_p}{dT_p} + R_pI_p + X_{c_p}\int I_p dT_p + \frac{d\psi_p}{dT_p} = \sin T_p \qquad (5.2)$$

Integrating Equations (5.1) and (5.2) and solving each for the magnetic flux linkages ψ_p, we get respectively:

$$-\psi_p = \cos T_p + L_pI_p + R_p\int I_p\, dT_p + \frac{1}{C_p}\iint I_p\, dT_p^2 \qquad (5.3)$$

or

$$-\psi_p = \cos T_p + X_{L_p}I_p + R_p\int I_p\, dT_p + X_{c_p}\iint I_p\, dT_p^2 \qquad (5.4)$$

The simulation of Equation (5.3) on the analogue computer is resolved into three parts:

(a) Non-linearity simulation,

(b) Periodic function generator simulation,

(c) Overall simulation.

---

*See Appendix C.

V.2.1 Non-linearity simulation.

To satisfy Equation (5.3) the analogue computer setup diagram of the non-linearity for the reactor is so chosen as shown in Figure 5.1*. The input-output curve of non-linearity is shown in Figure 5.2.

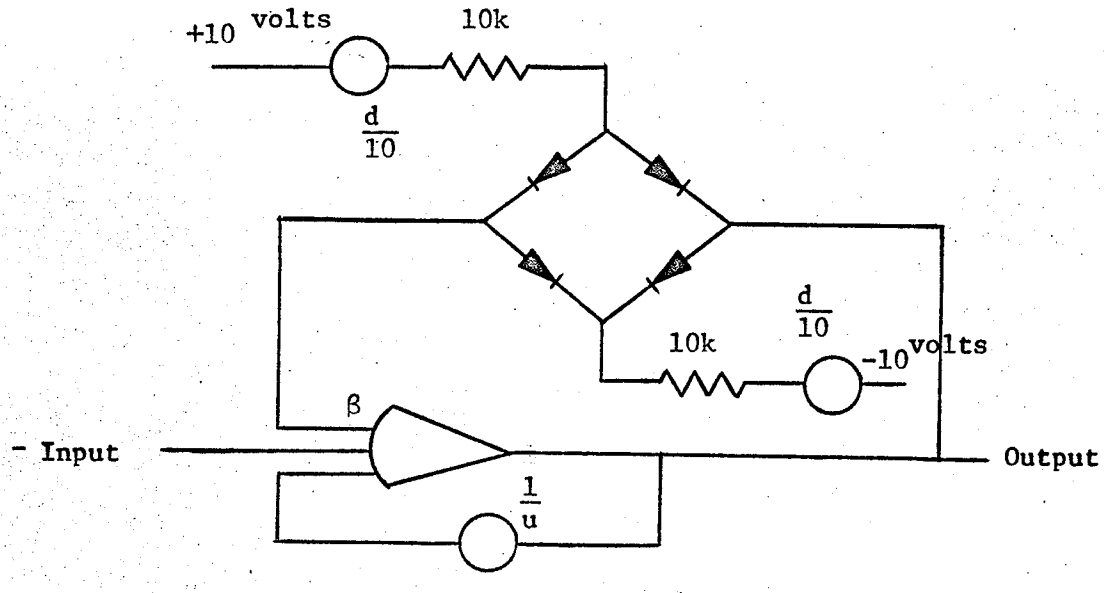

FIGURE 5.1 Non-linearity simulation

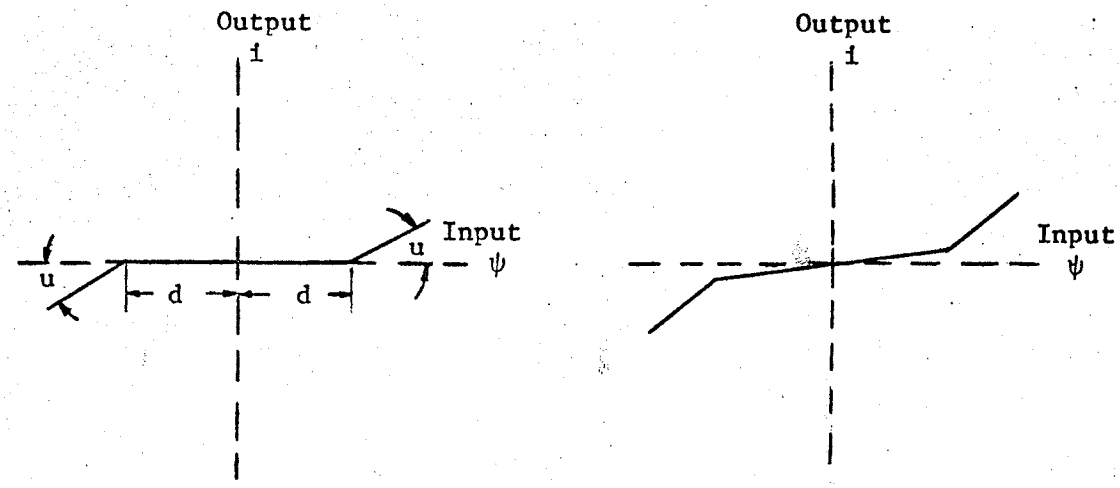

(a) Ideal Input-Output Curve (b) Actual Input-Output Curve.

FIGURE 5.2 Non-linearity for the Computer Setup Diagram of Figure 5.1.

---

*A list of analogue computer symbols is illustrated in Appendix D.1.

where d is the distance in per unit, and can be adjusted to any desired value.

u is the angle in radians, and can be adjusted to any desired value. When conducting, the diode introduces a low resistance to the feedback path, thus changing the gain of the operational amplifier. As a result, the dead space of the input-output curve has a slight slope as shown in Figure 5.2(b) which is absent in the input-output curve of Figure 5.2(a).

V.2.2 Periodic function generator simulations.

(a) Cosine generator simulation using 10-segment Variable Diode Function Generator (VDFG) method.

Figure 5.3 shows a typical cosine generator. Due to the leakage of the capacitors in the invertor and integrators, the accumulated drop of the voltage amplitude is appreciable if the cosine generator operates for more than five minutes. Subharmonic instability will result from this accumulated error. In order to overcome this defect, a 10-segment fix-break-point VDFG method is adopted. The computer setup diagram for the cosine generator (VDFG) is shown in Figure 5.4. The output of the VDFG is a cosine wave if the input is an isoceles triangular wave. (See Section V.2.2(b)).

(b) Isoceles triangular function generator simulation.

Figure 5.5 shows the computer setup diagram for the isoceles triangular function generator. The operation of the Electronic Associates, Inc. (EAI) electronic comparator of model 40.488 is such that no accumulated error occurs. The amplitude of the isoceles triangular generator remains constant during the operation. Coupling the output of the isoceles triangular generator to the input of the VDFG shown in Figure 5.4 gives a periodic

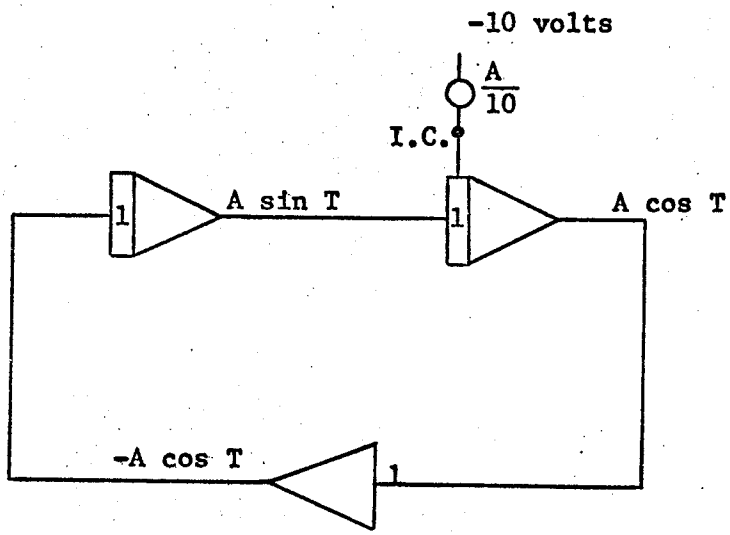

FIGURE 5.3 Typical Cosine Function Generator Setup Diagram.

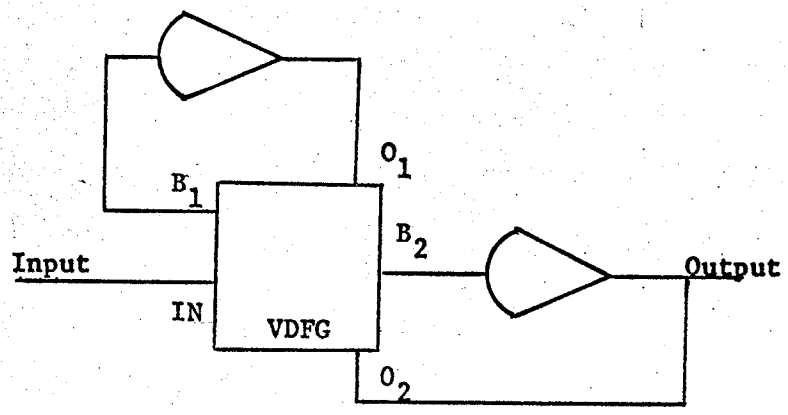

FIGURE 5.4 Cosine Function Generator Simulation Using VDFG Method.

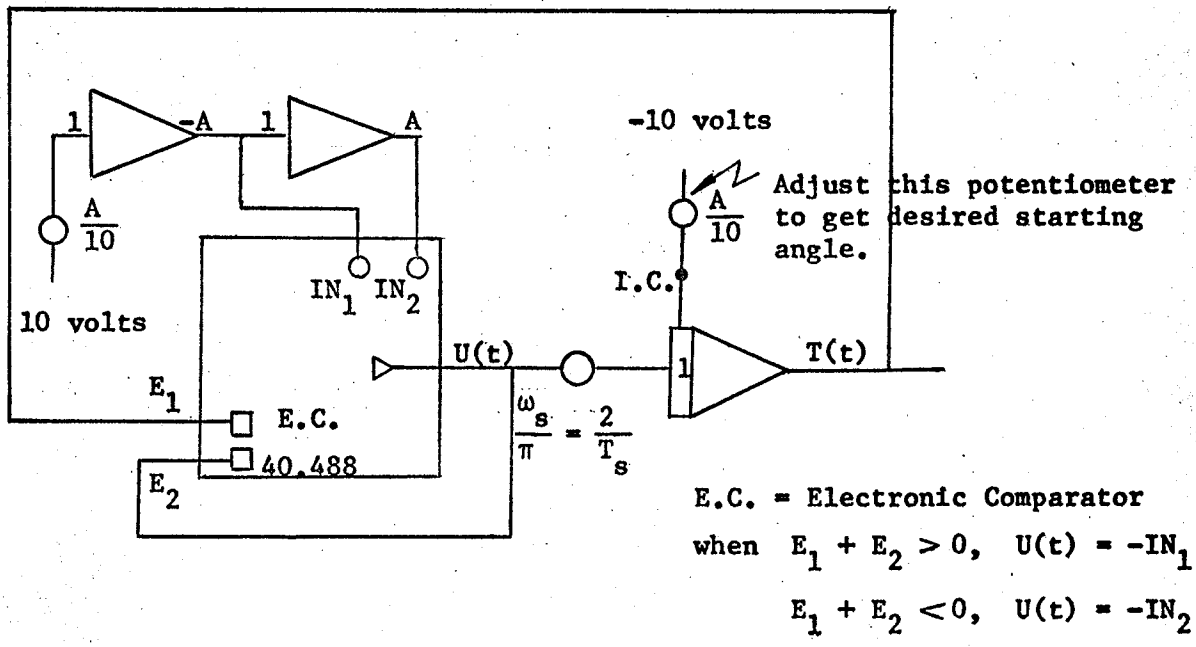

FIGURE 5.5(a) Isoceles Triangular Function Generator Setup Diagram

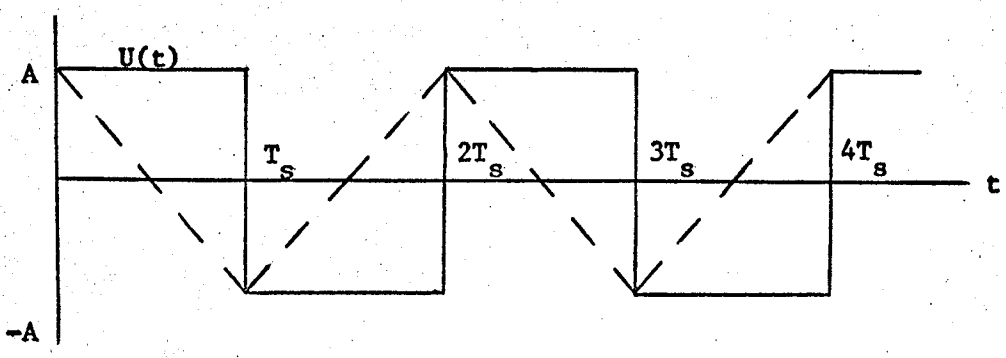

FIGURE 5.5(b) Isoceles Triangular and Square Waves.

cosine generator.

It should be noted that this cosine generator can start at any desired point of the voltage wave by adjusting the potentiometer to a suitable value. (See Figure 5.5(a)).

V.2.3 Over-all simulation.

The non-linearity and cosine wave generator simulations have been discussed. It is easy to simulate Equation (5.3) on the analogue computer. The basic analogue computer setup for the modified EHV ELD transmission line circuit is shown in Figure 5.6. The exact computer setup which was actually used is shown in Appendix D.2.

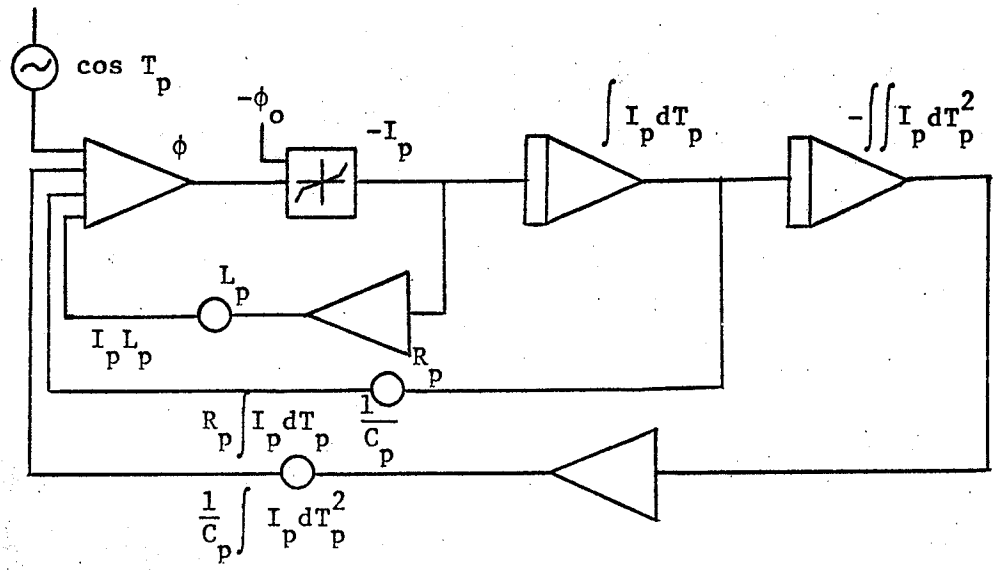

FIGURE 5.6 Analogue Computer Setup for the Modified EHV ELD Transmission Line Circuit.

The amplifier gains, and the potentiometer settings, are adjusted to correspond to particular values of the following variables:

(a) Magnitude of the applied voltage.

(b) Circuit parameters: Line inductance, Line resistance, Series capacitance, Saturation point (linear range) of the shunt reactor.

(c) Initial conditions: Initial capacitor charge Q_o, Initial flux linkages ψ_o, Switching angle θ_o.

V.3 Experimental Investigations.

It has been stated previously that a transient disturbance is necessary if subharmonic response is to be created. The switching transients caused by the zero point of the applied voltage wave, and transient overvoltages caused by the load rejection and the single-line-to-ground fault at no load were used to "shock" the circuit in the experiments.

V.3.1 Zero point of the applied voltage wave.

Extensive research[5, 11, 14] has been carried out to investigate the switching points of the applied voltage wave. The conclusion is that the point of switching with respect to voltage zero is a critical factor to create subharmonic oscillations. In accepting this, the voltage is closed at the zero point of the applied voltage wave. The other initial conditions and circuit parameters are:

Initial conditions: $Q_o = \psi_o = 0$

Circuit parameters: $L_p = 0.936$ per unit

$R_p = 0.04$ per unit

The linear range of the shunt reactor: $\psi_s = 1.2$ per unit and the applied voltage is: $E_m = 1.0$ per unit. The variation of the series compensation is from 0% (0 per unit) to 90% (0.844) at 10% step in each test.

No subharmonic was observed by closing the applied voltage at the zero point of the voltage wave in each test. But increasing the applied voltage to 1.4 per unit which is 0.4 per unit above the saturation point of the reactor, a second subharmonic was observed at 80% series compensation

$E_m = 1.4$ pu , $Q_o = \psi_o = \Theta_o = 0$, $\psi_s = 1.2$ pu

$X_c = .748$ pu , $L_p = 0.936$ pu , $R_p = 0.04$ pu

$= 80\%$

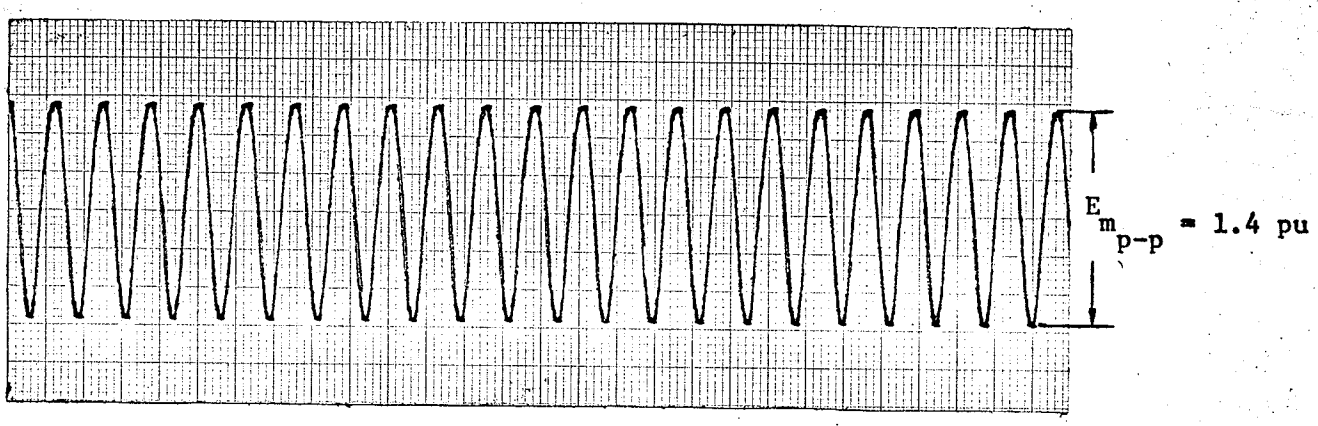

(a) Applied voltage

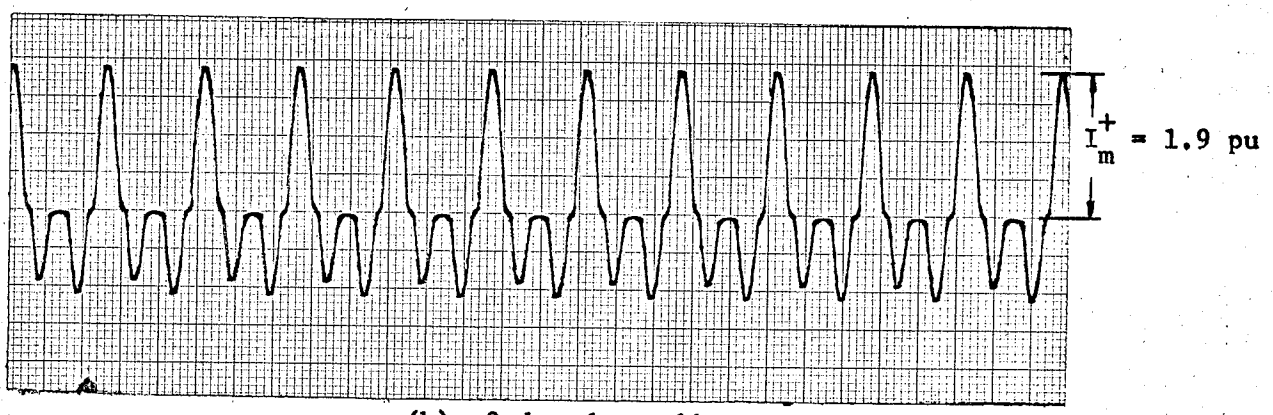

(b) 2nd order subharmonic current

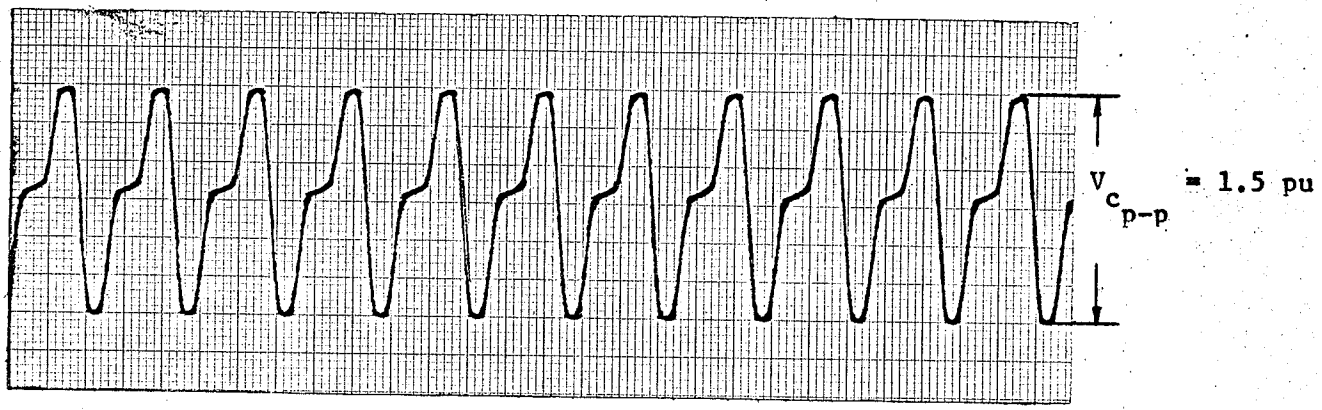

(c) Capacitance voltage

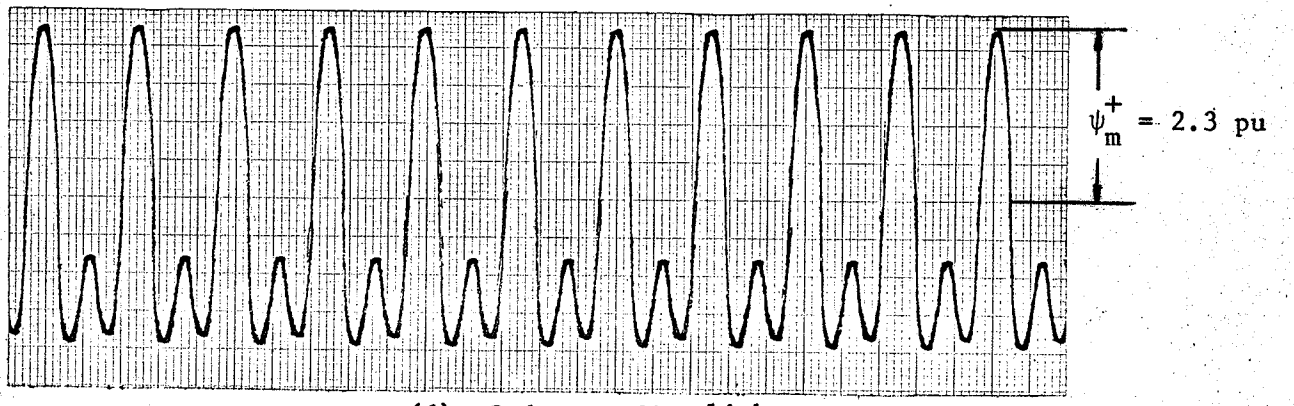

(d) Inductor flux linkages

FIGURE 5.7 Second Order Subharmonic Waveforms.

level. The waveforms are shown in Figure 5.7. It can be seen that serious overvoltage on the capacitor is a result of subharmonic response.

V.3.2 Load rejection and single-line-to-ground fault.

The transient overvoltages resulting from load rejection and single-line-to-ground fault at no load are represented by placing two per unit initial flux linkages on the reactor.[6] The existence of subharmonic oscillations as the series compensation is varied and the avoidance of subharmonic oscillations as the linear range of the magnetic characteristic of the shunt reactor is varied are viewed as follows:

(a) Variation with series compensation.

The second order and the third order subharmonics observed as the series compensation is varied are illustrated in Table V.1. The initial conditions and circuit parameters are as follows:

Initial Conditions: $Q_o = 0$

θ_o = arbitrary

$\psi_o = 2$ per unit

Circuit parameters: $L_p = 0.936$ per unit

$R_p = 0.04$ per unit

$\psi_s = 1.2$ per unit

and the applied voltage is: $E_m = 1$ per unit.

It can be seen from Table V.1 that there are distinct areas where these subharmonics occur. The third order subharmonic is present to the greatest extent. The second order subharmonic occurs only at a very high series compensation level. No further study has been made to investigate the subharmonic oscillations when the series compensation is greater than 90%.

TABLE V.1. Variation of Subharmonic Orders with Series Compensation.

	No Subharmonic					3rd order subharmonic			2nd order subharmonic	
X_c (percentage)	0	10%	20%	30%	40%	50%	60%	70%	80%	90%
X_c (per unit)	0	.0935	.187	.281	.375	.468	.562	.655	.748	.844

A check with the formula (3.5) used to predict the regions where the various orders of subharmonics occur is as follows:

For the second subharmonic:

$$X_{c_p} = 0.748 \text{ per unit}, \qquad R_p = 0.04 \text{ per unit}$$

$$\delta = \frac{0.04}{0.748} = 0.0539$$

For the third order subharmonic:

$$X_{c_p} = 0.468 \text{ per unit}, \qquad R_p = 0.04 \text{ per unit}$$

$$\delta = \frac{0.04}{0.0468} = 0.0855$$

These values of relative loss factor fall in the predicted regions[4] between $\delta = 0$ to $\delta_c = 0.1$ and $\delta = 0$ to $\delta_c = 0.3$ for the occurrence of the second order and third order subharmonics respectively.

Figure 5.8 shows that the third order subharmonic current and capacitor voltage decrease with the increase of series compensation level. When the second order subharmonic occurs, the current and the capacitor voltage suddenly jump to very high magnitudes. With a further increase of series compensation level, a little decrease of current and capacitor voltage

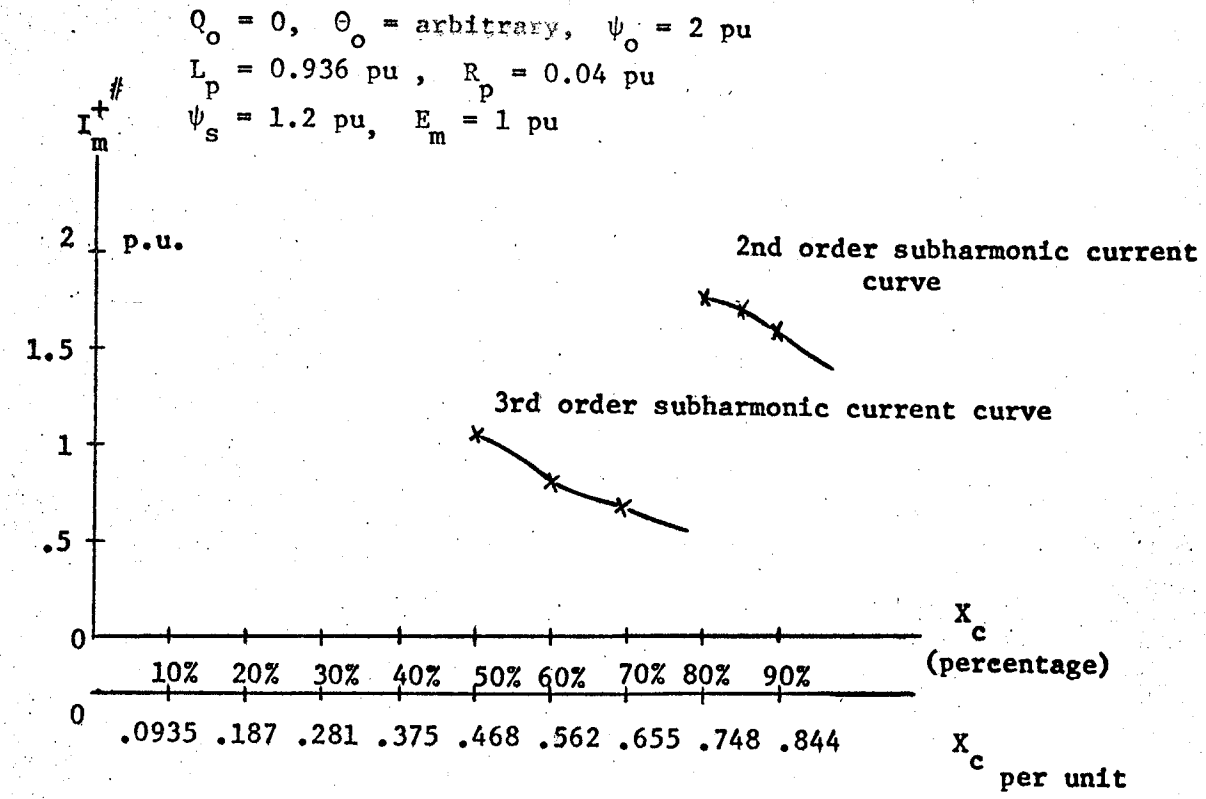

FIGURE 5.8(a) Variation of the Magnitude of Subharmonic Currents with Series Compensation.

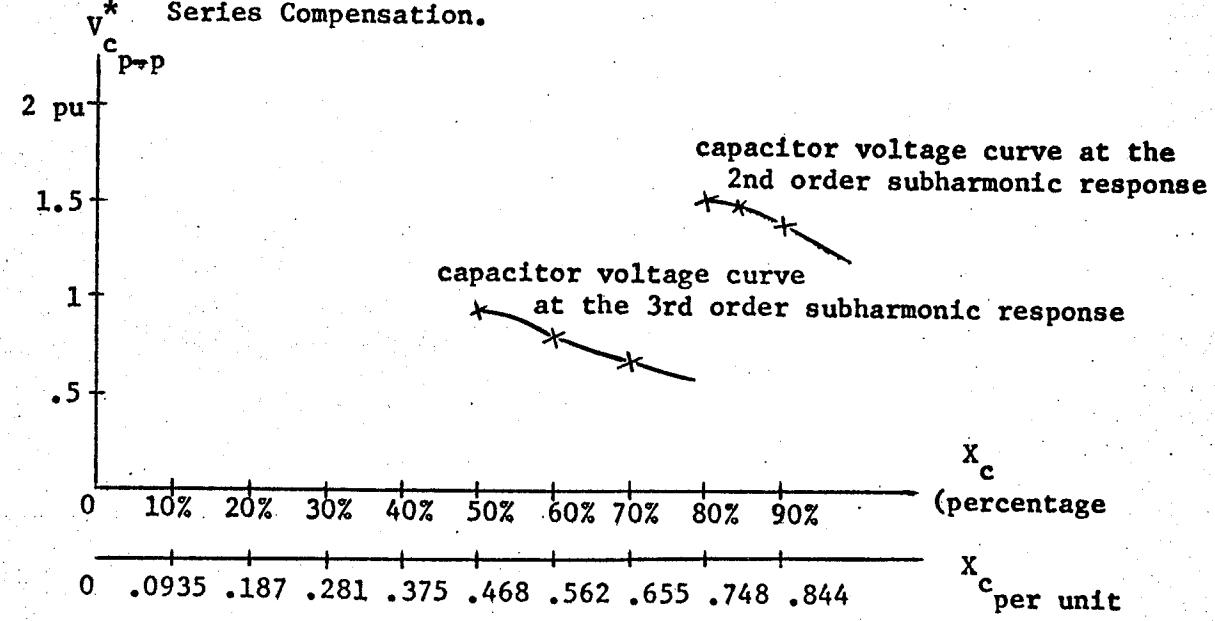

FIGURE 5.8(b) Variation of the Magnitude of Capacitor Voltages with Series Compensation.

---

* $V_{c_{p-p}}$ = Peak to peak value of capacitor voltage

I_m^+ = Positive maximum value of subharmonic current.

E_m = 1 pu , Q_o = 0 , ψ_o = 2 pu , ψ_s = 1.2 pu , Θ_o = arbitrary

X = .748 pu , R_p = 0.04 pu , L_p = 0.936 pu .

= 80%

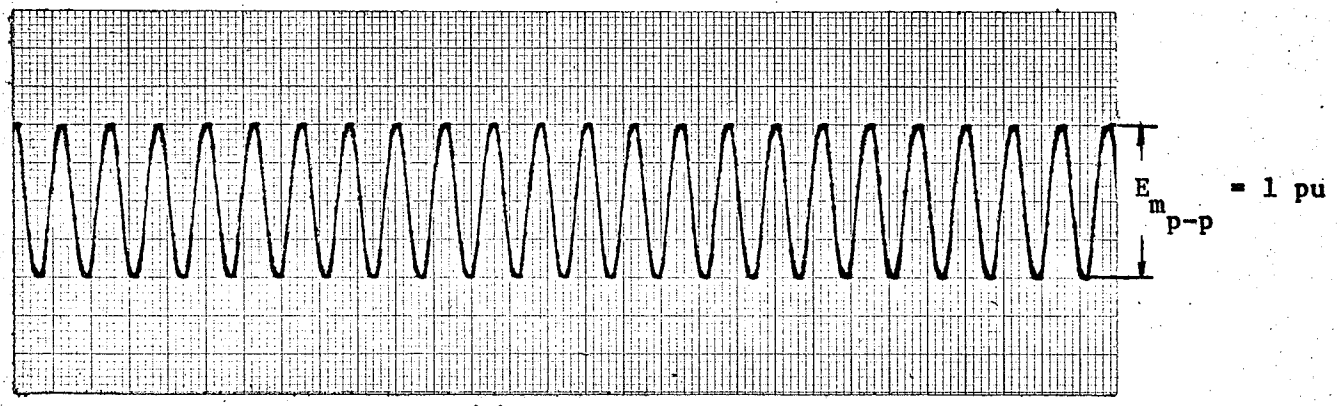

(a) Applied voltage

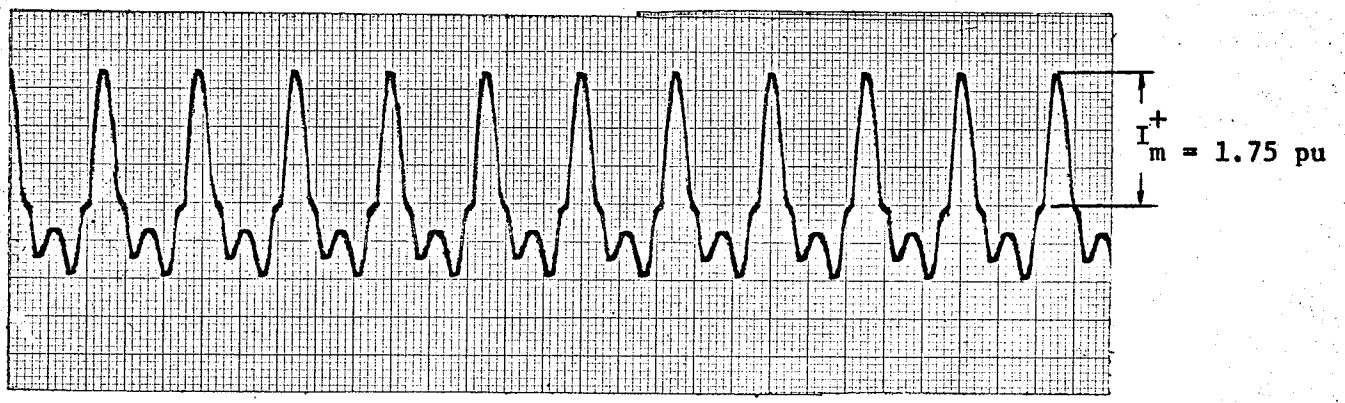

(b) 2nd order subharmonic current

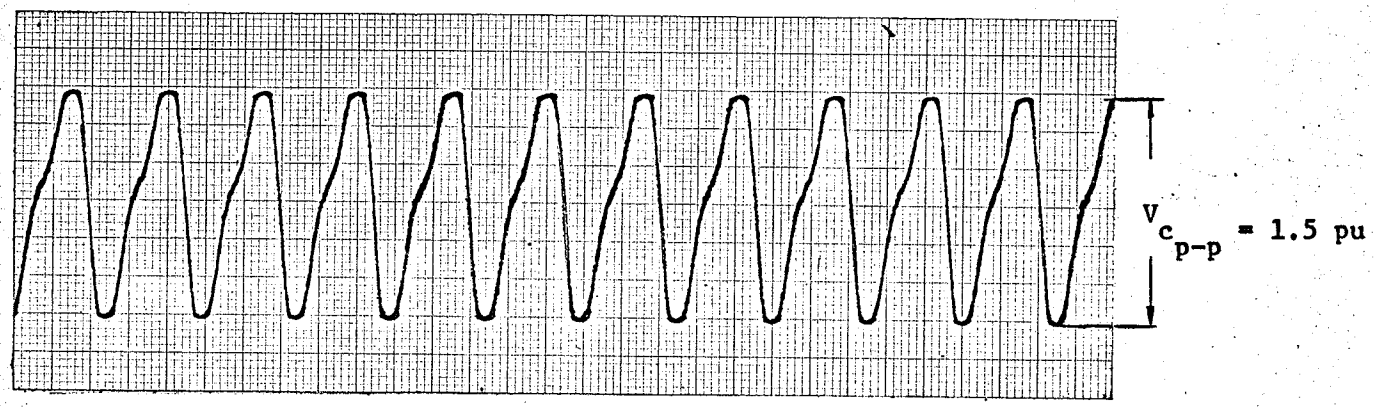

(c) Capacitor Voltage

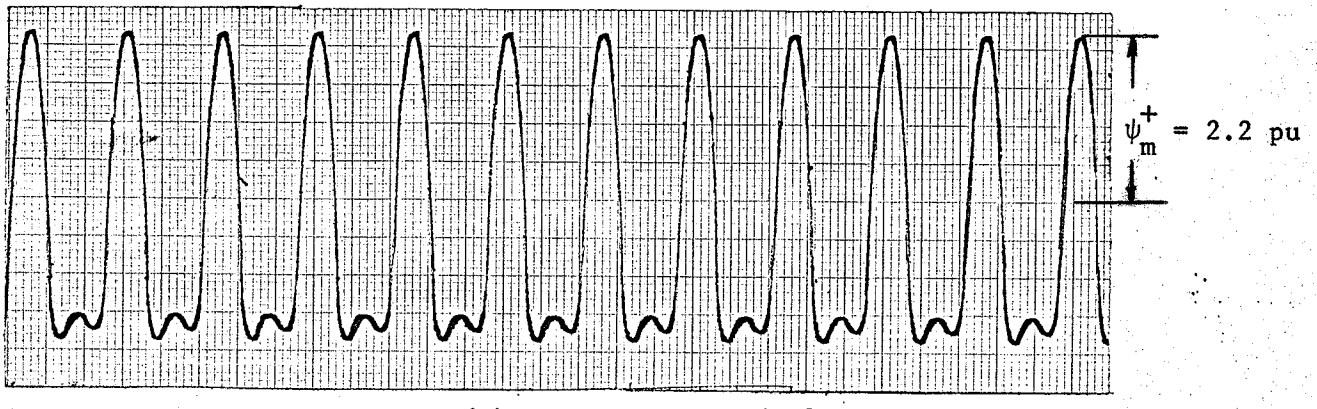

(d) Inductor flux linkages

FIGURE 5.9. Second Order Subharmonic Waveforms.

E_m = 1 pu , Q_o = 0 , Θ_o = arbitrary , ψ_o = 2 pu , ψ_s = 1.2 pu ,

X_c = .468 pu , R_p = 0.04 pu , L_p = 0.936 pu ,

= 80%

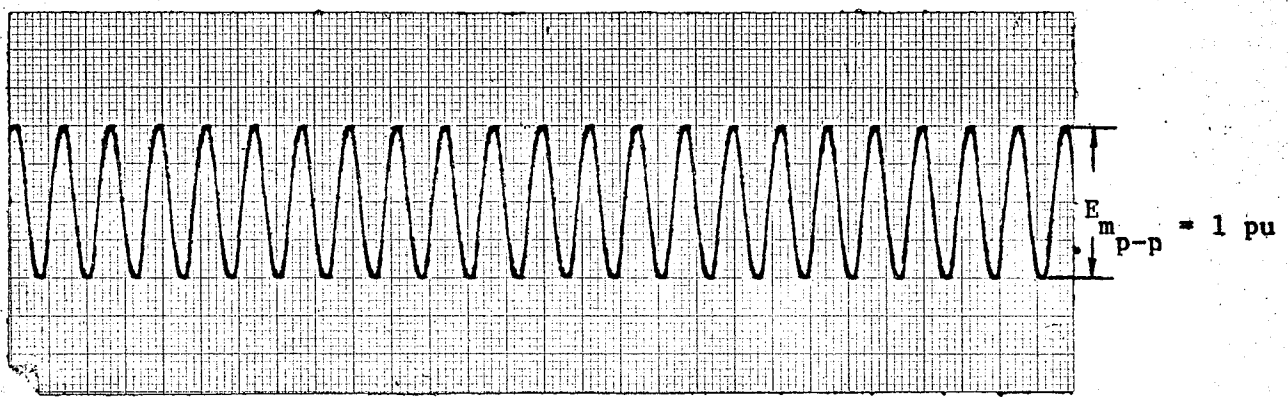

(a) Applied voltage

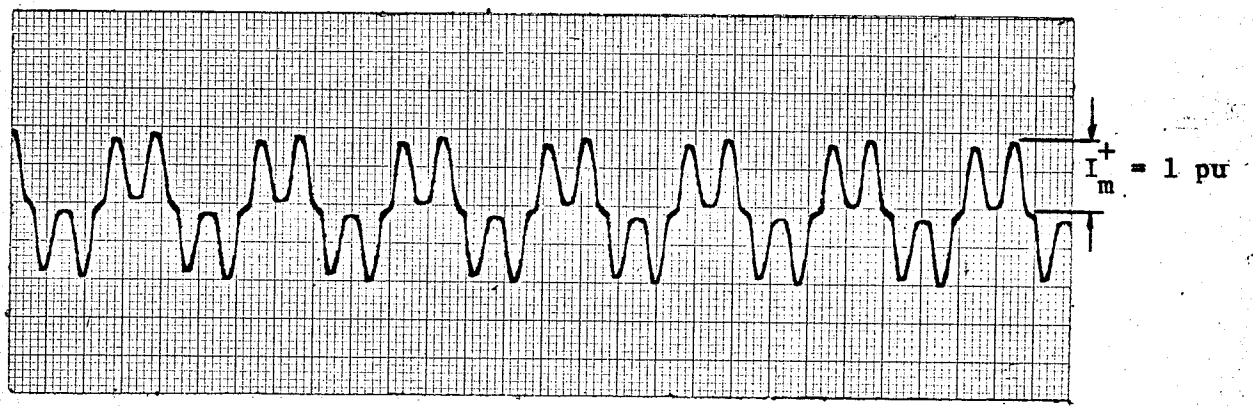

(b) 3rd subharmonic current

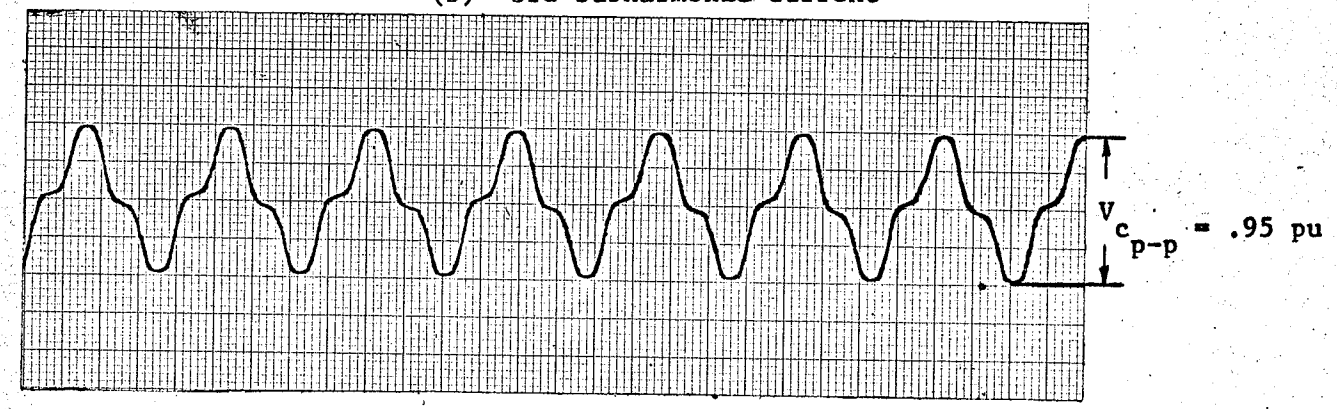

(c) Capacitor voltage

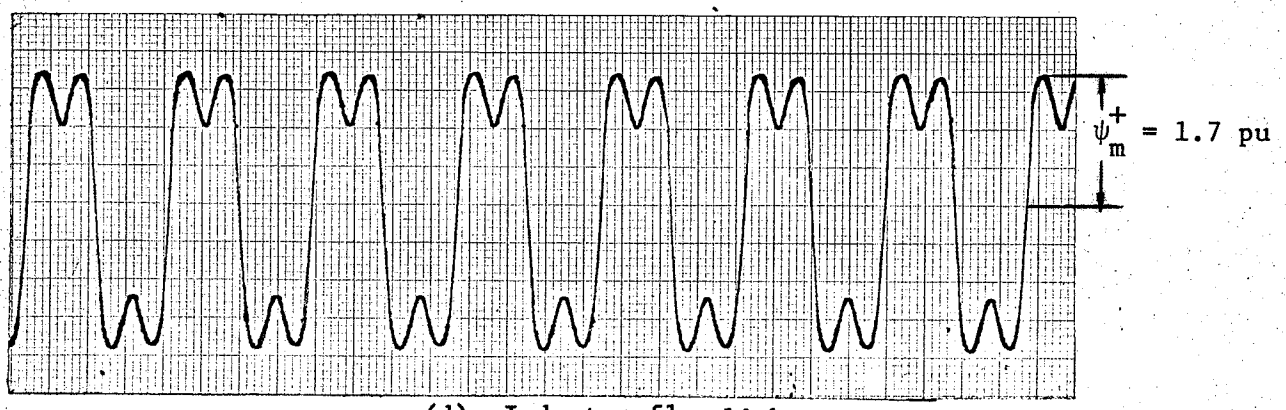

(d) Inductor flux linkages

FIGURE 5.10 Third Order Subharmonic Waveforms.

will result. The numerical data of the second order and the third order subharmonics are listed in Appendix E.1.

Figure 5.9 and Figure 5.10 show the waveforms of the second and the third order subharmonic oscillations respectively.

(b) Variations with the linear range of the shunt reactor.

The existence of the second order and the third order subharmonics at 1 per unit linear range of the magnetic characteristic of the shunt reactor, for different levels of series compensation is illustrated in Figure 5.11. (The numerical data are listed in Appendix E.2) and Table V.2. The initial conditions and other circuit parameters are:

Initial conditions $Q_o = 0$

Θ_o = arbitrary

$\psi_o = 2$ per unit

Circuit parameters: $L_p = 0.936$ per unit

$R_p = 0.04$ per unit

$\psi_s = 1.0$ per unit

and the applied voltage is: $E_m = 1$ per unit.

A study of Table V.1 and Table V.2 indicates that the second and third order subharmonics occur at a lower series compensation level for a shorter linear range of the magnetic characteristic of a shunt reactor. Comparing Figure 5.8 and Figure 5.11 also indicates that the magnitudes of subharmonic currents and capacitor voltages are higher for a shorter linear range of the magnetic characteristic of a shunt reactor at subharmonic oscillations.

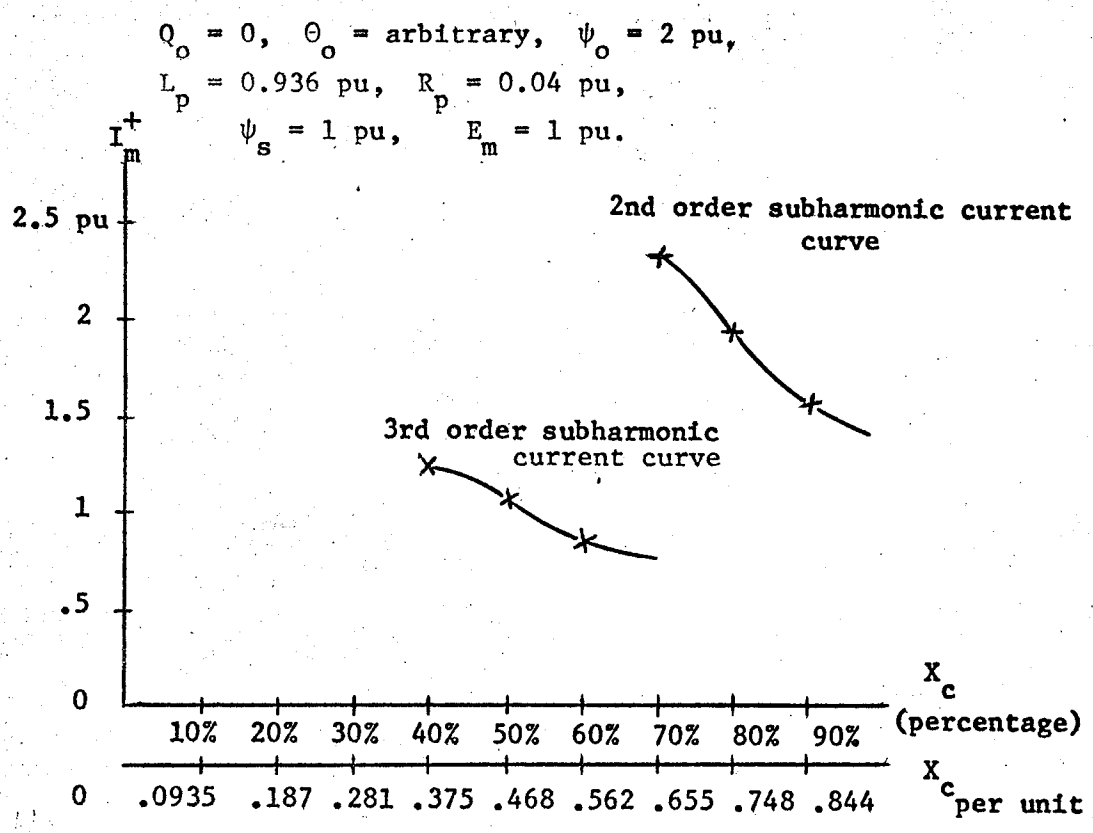

FIGURE 5.11(a) Variation of the Magnitude of Subharmonic Currents with Series Compensation.

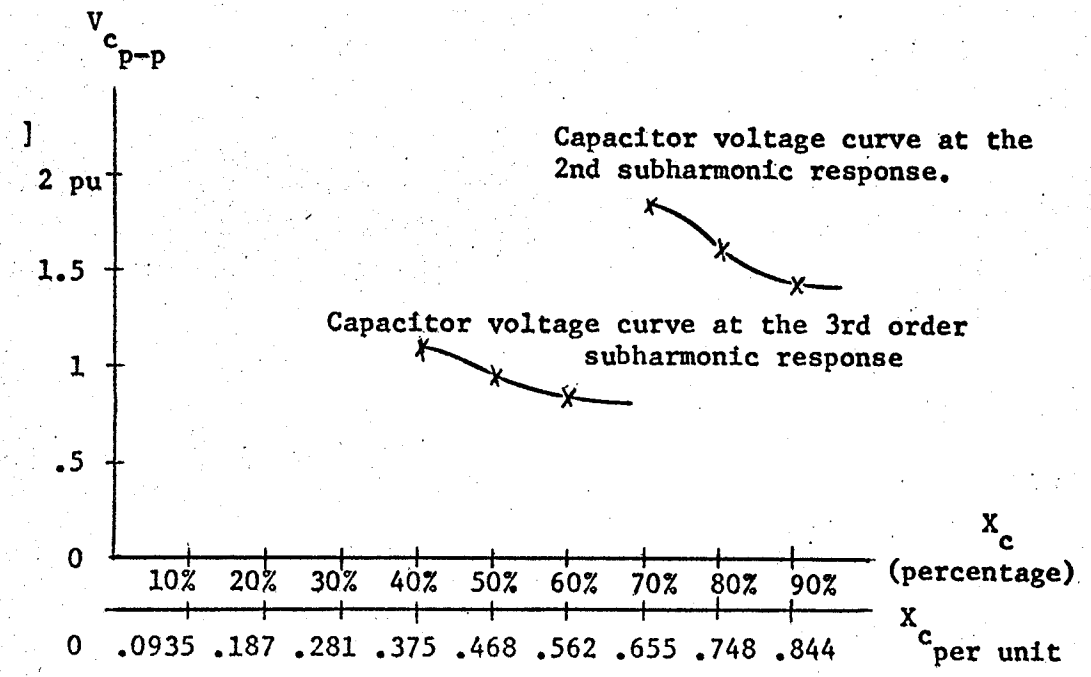

FIGURE 5.11(b) Variation of the Magnitude of Capacitor Voltages with Series Compensation.

TABLE V.2 Variation of Subharmonic Orders with Series Compensation.

	no subharmonic			3rd order subharmonic			2nd order subharmonic		
X_c (percentage)	0	10%	20% 30%	40%	50%	60%	70%	80%	90%
X_c (per unit)	0	.0935	.187 .281	.375	.468	.562	.655	.748	.844

Figure 5.12 illustrates that the subharmonic current decreases with the increase of the linear range of the magnetic characteristic of the shunt reactor. No subharmonic will occur if the linear range of the magnetic characteristic of the shunt reactor is higher than 1.5 per unit. (The numerical data are presented in Appendix E.3).

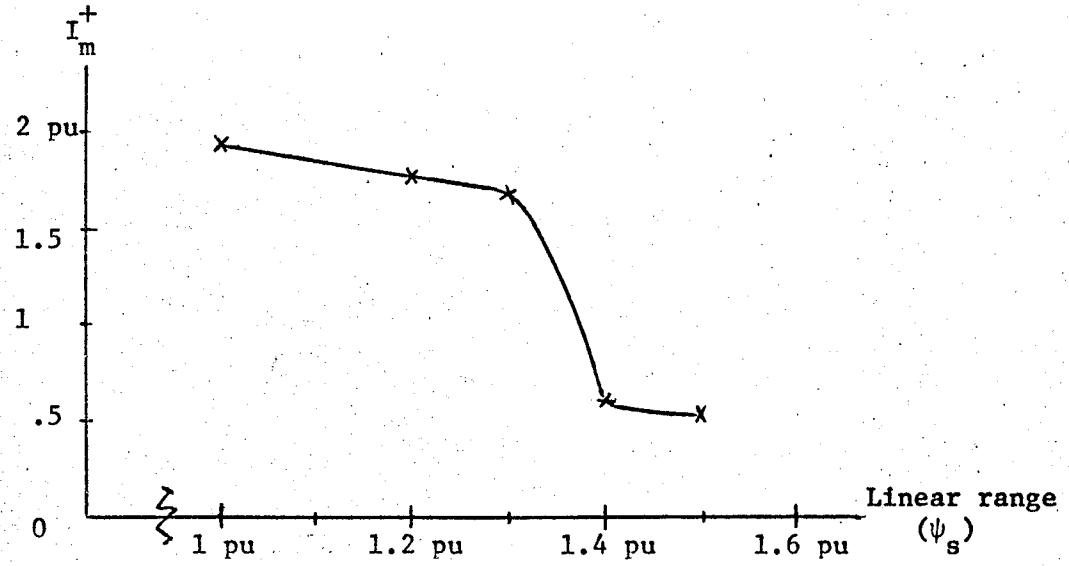

FIGURE 5.12 Variation of Magnitude of Subharmonic Current with Linear Range of the shunt Reactor

$Q_o = 0$, Θ_o = arbitrary, $\psi_o = 2$ per unit ,

$L_p = 0.936$ per unit, $R_p = 0.04$ per unit,

$\frac{1}{C_p} = 0.748$ per unit, $E_m = 1$ per unit.

V.4 Summary

It has been demonstrated that the modified transmission line circuit can be simulated on the analogue computer for the purpose of studying the existance of subharmonic oscillations under various conditions. The results obtained are valid and important even though line susceptance was neglected.

The switching transients caused by closing the breaker at no load or at light load may create subharmonic oscillations. But, if the shunt reactor is designed to have a sufficiently high linear range, no subharmonic will occur.

The transient overvoltages caused by load rejection and single-line-to-ground fault at no load may "shock" the system to create subharmonic oscillations. But these subharmonic oscillations can be avoided by suitably dimensioning the linear range of the magnetic characteristic of the shunt reactor.

CHAPTER V

ANALOGUE COMPUTER SIMULATION

It has been stated in CHAPTER II that transient overvoltages will result from switching, load rejection and single-line-to-ground fault at no load. The switching transients caused by closing the breaker(s) at no load or light load may create subharmonic response. The transient overvoltages caused by load rejection and single-line-to-ground fault at no load may "shock" a transmission line to create subharmonic oscillations. In this chapter, a series of experiments is carried out on the analogue computer* to answer the following questions:

(a) Can subharmonics occur at a high series compensation level?

(b) If switching takes place at the zero point of the applied voltage wave, will a subharmonic occur?

(c) How does the linear portion of the magnetic characteristic of a shunt reactor affect the occurrence of subharmonic?

V.1 System Study.

An EHV ELD transmission system schematic diagram is shown in Figure 2.1, page 13. The transmission line to be investigated is 600 miles long, at a 500 KV service voltage. The sending and receiving end transformers and the sending end generators are not included. The line and series compensation data are listed as follows:

---

*The computer which was used is the ELECTRONIC ASSOCIATES, INC. (EAI) of model TR-48.

subharmonic with a magnitude greater than that of the third order subharmonic will be created.

In conclusion, the answers for the questions posed in the Introduction (pages 1 and 2) may be stated as follows:

(1) Subharmonic oscillations are of high-magnitude, low frequency type, with the frequencies a fraction of that of the applied voltage. Under very limited conditions, subharmonic oscillations may occur if a "shock" or a "transient" is introduced into the non-linear circuit.

(2) Usually, high series compensation level is more susceptible to subharmonic oscillations. (See Tables I and II, pages 53 and 59 respectively).

(3) When subharmonic resonance does occur, the magnitude of the line current and capacitor voltage is found to be very high in comparison with that of the "normal magnetizing current" state, i.e. the state of normal operation.

(4) Subharmonic oscillations can be controlled or eliminated by the proper selection of the circuit parameters, such as E_m, R, L, C and ψ_s -- the linear portion of the magnetic characteristic of a shunt reactor.

APPENDIX A

A MODIFIED CIRCUIT OF AN EHV ELD TRANSMISSION LINE

A.(a). Investigation of a Shunt Reactor.

The equivalent circuit and the model of a shunt reactor[4] are shown in Figure A.1(a) and A.1(b) respectively. The current flowing through the reactor is:

$$I_T = I_a + I_c \tag{A.1}$$

where I_T is the total current flowing through the reactor,

I_a is the branch current flowing through the air gap inductance,

I_c is the branch current flowing through the core inductance.

and the flux linkages of the reactor are:

$$\psi_T = \psi_c + \psi_\ell \tag{A.2}$$

where ψ_T is the total flux linkages of the reactor,

ψ_c is the flux linkages of the core or of the air gap,

ψ_ℓ is the flux linkages of the leakage path outside the core.

Equation (A.2) may be written as:

$$\psi_T = L_a I_a + L_\ell I_T \tag{A.3.a}$$

or

$$\psi_T = L_c I_c + L_\ell I_T \tag{A.3.b}$$

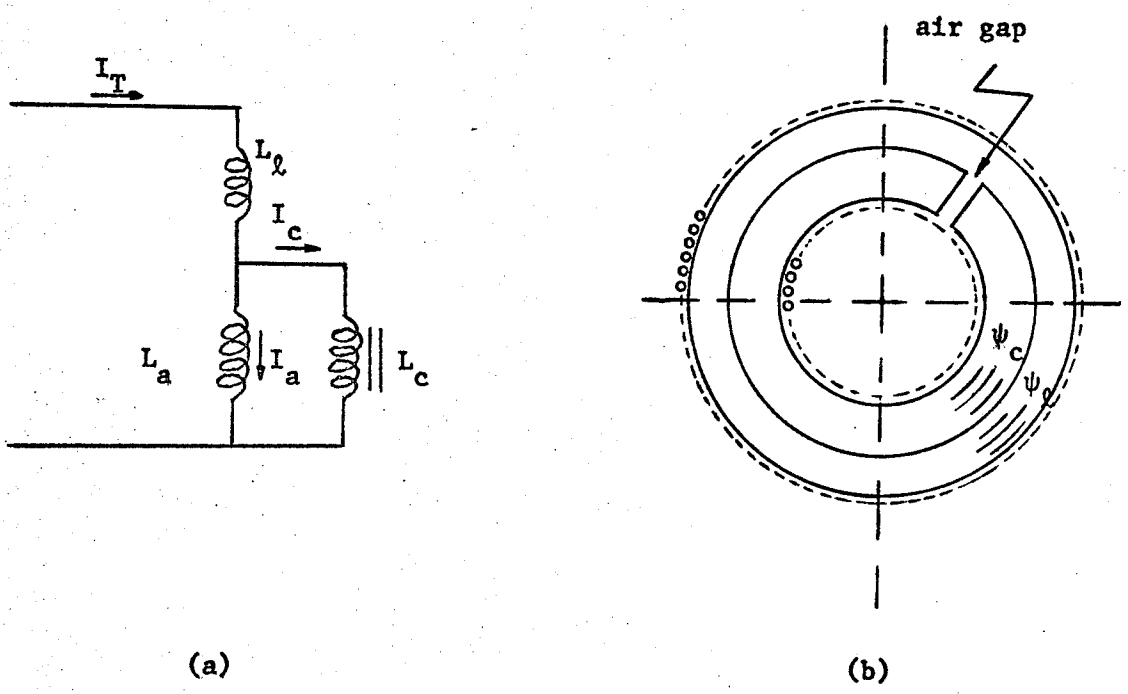

FIGURE A.1 Shunt Reactor (a) Equivalent circuit, (b) Model.

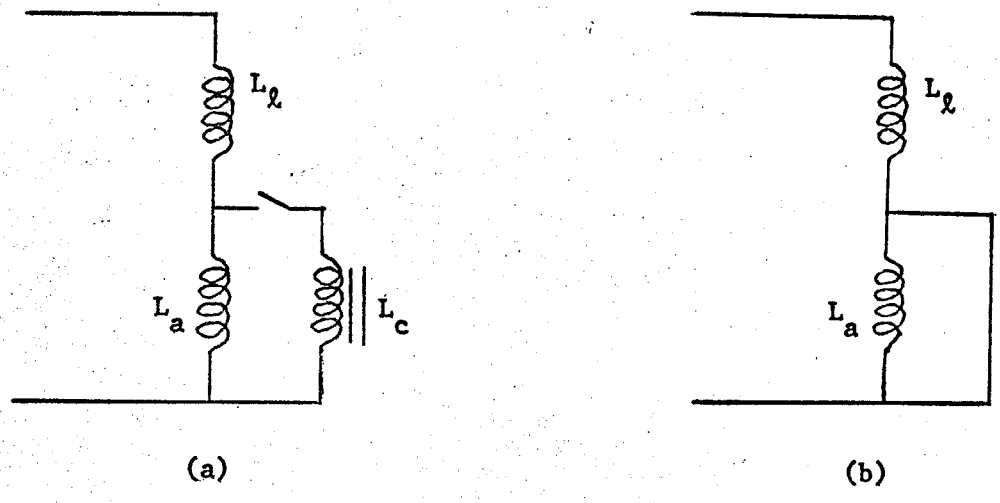

FIGURE A.2 Behaviour of a Shunt Reactor. (a) Before saturation, (b) High saturation.

where L_a is the air-gap inductance,

L_c is the core inductance ,

L_ℓ is the leakage inductance.

Fortunately, L_a and L_ℓ are linear, only L_c is non-linear. Before saturation, L_c is very high and is very low after saturation. In practice, L_c may be assumed to be "ideal" by letting L_c equal infinity (open circuit) before saturation and zero (short circuit) at high saturation. (See Figure A.2). As a result, the inductance of the shunt reactor before saturation is:

$$L_1 = L_\ell + L_a \qquad \text{(A.4.a)}$$

and at high saturation is:

$$L_2 = L_\ell \qquad \text{(A.4.b)}$$

Usually L_2 is very low in comparison with L_1. Relating L_1 and L_2 gives:

$$L_2 = \frac{1}{K} L_1 \qquad \text{(A.5)}$$

where K is a constant.

An experimental investigation[11, 16] has shown that L_2 is at least ten times less than L_1.

A.(b). The Equivalent Circuit.

The equivalent circuit of an ELD transmission line with series and shunt compensations is shown in Figure A.3, where the sending end voltage is

shown, and the receiving end is open-circuited.

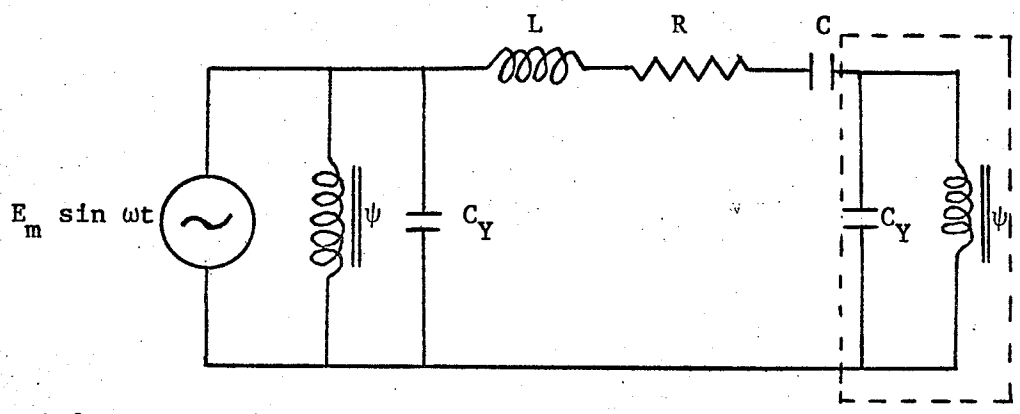

FIGURE A.3. Equivalent π Circuit with Series and Shunt Compensations.

Before the investigation, it may be of interest to see the change of the reactance of a shunt reactor relative to the lumped capacitive reactance of the line before and after the occurrence of a subharmonic response.

Consider the reactor shunted with the lumped capacitance C_Y of the line as bounded by the dotted line in Figure A.3. It has been stated that the inductances of the shunt reactor are L_1 and L_2 before saturation and at high saturation respectively. At system frequency ω (before saturation), the ratio of X_Y to X_1 is:

$$\frac{X_Y}{X_1} = \frac{\frac{1}{\omega C_Y}}{\omega L_1} \qquad (A.6)$$

where X_Y is the lumped capacitive reactance of the line

and X_1 is the reactance of the shunt reactor before saturation.

For the nth order subharmonic response (high saturation) the system frequency is $\frac{1}{n}\omega$. The ratio of the lumped capacitive reactance of the line to the reactance of a shunt reactor is:

$$\frac{X'_Y}{X_2} = \frac{\frac{1}{\frac{1}{n}\omega C_Y}}{\frac{1}{n}\omega L_2} \qquad (A.7)$$

where X_2 is the reactance of the shunt reactor at high saturation. Substituting Equations (A.5) and (A.6) into Equation (A.7) yields:

$$\frac{X'_Y}{X_2} = \frac{nX_Y}{\frac{1}{m_o}X_1} \qquad (A.8)$$

where $m_o = K n$

Equation (A.8) illustrates that the lumped capacitive reactance of the line is n times larger, while the reactance of the shunt reactor is $\frac{1}{m_o}$ times smaller at the nth order subharmonic response.

Example:

Consider the Figure A.3 for the second order subharmonic response, then $n = 2$ and in Appendix A(a) $K = 10$. Therefore, from Equation (A.8) we obtain:

$$\frac{X'_Y}{X_2} = \frac{2X_Y}{\frac{1}{2\times 10}X_1} = 40\frac{X_Y}{X_1} \qquad (A.9)$$

In an EHV ELD transmission line, the shunt compensation is so designed that the reactance of a shunt reactor is approximately equal to or less than the lumped capacitive reactance of the line at applied voltage frequency (ω). For the sake of simplicity, let $X_Y = X_1$, then Equation (A.9) becomes:

$$\frac{X'_Y}{X_2} = 40$$

or

$$X'_Y = 40\ X_2$$

This means that the lumped capacitive reactance of the line is 40 times that of the reactance of the shunt reactor at the second order subharmonic response. As a result, it is reasonable to neglect the lumped capacitve reactance which is in parallel with the reactance of the shunt reactor at subharmonic oscillations.

A.(c). The Modified Circuit.

Since the lumped capacitive reactances at both the sending and receiving ends are neglected in the study of subharmonic oscillations, Figure A.3 can be modified to that shown in Figure A.4 below:

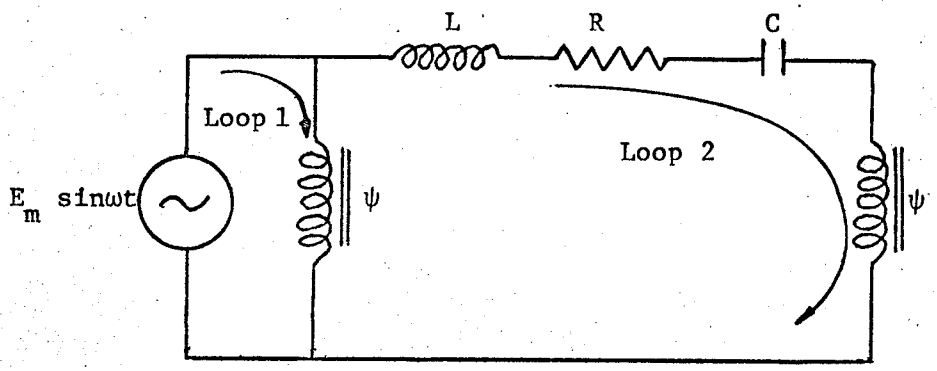

FIGURE A.4. Equivalent Transmission Line Circuit by Neglecting the Lumped Capacitive Reactances.

A study of Figure A.4 reveals that the current circulating through the sending end reactor as indicated loop 1, is insignificant. Only the current flowing through the series capacitors to the receiving end is of special interest. Thus a further modification of the transmission line circuit

for the purpose of analysing the subharmonic oscillations is given in Figure A.5.

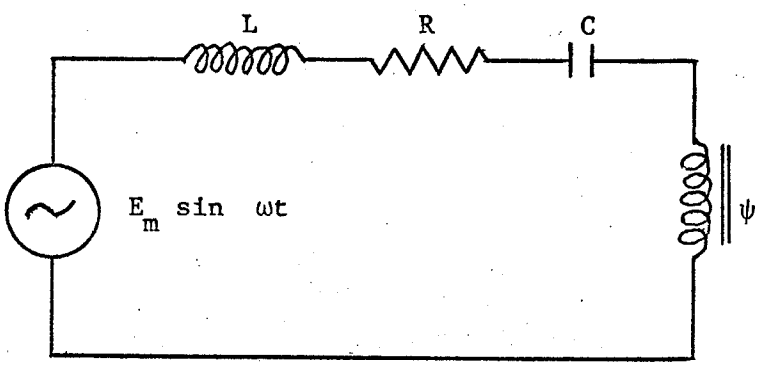

FIGURE A.5 A Modified Circuit of an EHV ELD Transmission Line with Sending Voltage.

APPENDIX B

CALCULATIONS OF THE LINE REACTANCE AND THE LINE SUSCEPTANCE

The conductor used for this study is a 4-bundle conductor of 795000 circular mils with $54x7$ strands. The construction of the tower is a flat configuration. The separation between the adjacent subconductors is 1.5 feet, and the spacing between the phases is 35 feet.

The formulae used for calculating the line reactance and the lumped capacitive reactance of a transmission line are as follows:

The line reactance of a four-bundle conductor is:

$$X_L^+ = \frac{1}{4} (X_a - 3X_s) - 0.0106 \left(\frac{f}{60} \right) + X_d \qquad (B.1)$$

in which

$$X_a = 0.2794 \left(\frac{f}{60} \right) \log \frac{1}{GMR}$$

$$X_s = 0.2794 \left(\frac{f}{60} \right) \log S$$

$$X_d = 0.2794 \left(\frac{f}{60} \right) \log GMD.$$

and the lumped capacitive reactance of a four-bundle conductor is:

$$X_Y^+ = \frac{1}{4} (X_a' - 3X_s') - 0.0026 \left(\frac{60}{f} \right) + X_d' \qquad (B.2)$$

in which

$$X'_a = 0.0683 \left(\frac{60}{f}\right) \log \frac{1}{r}$$

$$X'_x = 0.0683 \left(\frac{60}{f}\right) \log S$$

$$X'_d = 0.0683 \left(\frac{60}{f}\right) \log GMD$$

where X_L^+ is the positive sequence reactance expressed in ohm per mile per phase

X_Y^+ is the positive sequence lumped capacitive reactance expressed in ohm per mile per phase

f is the service voltage frequency (Hz)

S is the separation of the adjacent subconductors expressed in feet

r is the radius of the subconductor expressed in feet

GMR is the geometric mean radius of the subconductor expressed in feet

GMD is the geometric mean distance between the centre line of the phases expressed in feet.

APPENDIX C

PER UNIT QUANTITIES

The differential equation for the modified transmission line circuit is:

$$L\frac{di}{dt} + Ri + \frac{1}{C}\int idt + \frac{d\psi}{dt} = E_m \sin \omega t \qquad (C.1)$$

Equation (C.1) can be written as:

$$X_L\frac{di}{d\omega t} + Ri + X_c\int id\omega t + \frac{\omega d\psi}{d\omega t} = E_m \sin \omega t \qquad (C.2)$$

where $X_L = \omega L$ and $X_c = \frac{1}{\omega C}$

A set of base units (i.e. E_b, I_b, T_b) is so chosen that:

$$E_b = E_m, \quad I_b = I_m, \quad T_b = \frac{1}{\omega}$$

and let

$$Z_b = \frac{E_b}{I_b} = \frac{\omega\psi_b}{I_b} = \omega L_b = \frac{1}{\omega C_b}$$

Dividing Equation (C.2) by E_b and rearranging yields:

$$\frac{X_L}{Z_b}\frac{d(i/I_b)}{d(t/T_b)} + \frac{Ri}{Z_b I_b} + \frac{X_c}{X_b}\int \frac{i}{I_b}\, d\left(\frac{t}{T_b}\right) + \frac{d(\psi/\psi_b)}{d(t/T_b)} = \sin\frac{t}{T_b} \qquad (C.3)$$

Substituting

$$\frac{X_L}{Z_b} = \frac{L}{L_b} = X_{L_p} = L_p^*$$

$$\frac{X_c}{X_b} = \frac{1}{C/C_b} = X_{c_p} = \frac{1}{C_p}$$

$$\frac{R}{Z_b} = R_p, \quad \frac{I}{I_b} = I_p, \quad \frac{\psi}{\psi_b} = \psi_p$$

and

$\frac{t}{T_b} = T_p$ into Equation (C.3) yields:

$$L_p \frac{dI_p}{dT_p} + R_p I_p + \frac{1}{C_p} \int I_p \, dT_p + \frac{d\psi_p}{dT_p} = \sin T_p$$

or

$$X_{L_p} \frac{dI_p}{dT_p} + R_p I_p + X_{c_p} \int I_p \, dT_p + \frac{d\psi_p}{dT_p} = \sin T_p$$

---

* The subscript "P" means per unit.

APPENDIX D

COMPUTER SYMBOLS AND EXACT COMPUTER SETUP DIAGRAM

D.1 LIST OF SYMBOLS

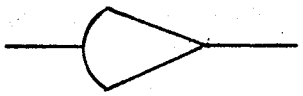

Operational amplifier

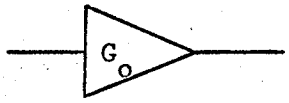

Invertor or amplifier with indicated gain.

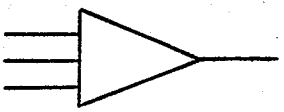

Summer

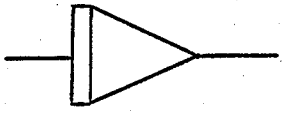

Integrator

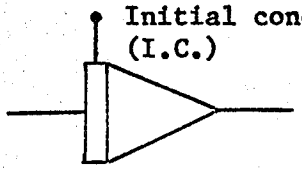

Integrator with I.C.

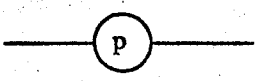

Potentiometer of ratio p

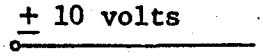

± 10 volts d.c. reference source

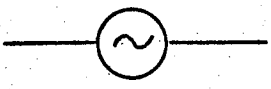

Cosine generator

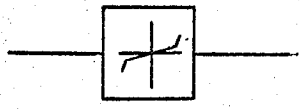

Non-linear device with indicated transfer function

Diode

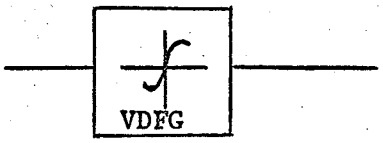

VDFG with indicated periodic generator

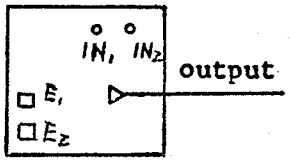

Electronic comparator

D.2 Exact Computer Setup Diagram for an EHV ELD Transmission Line

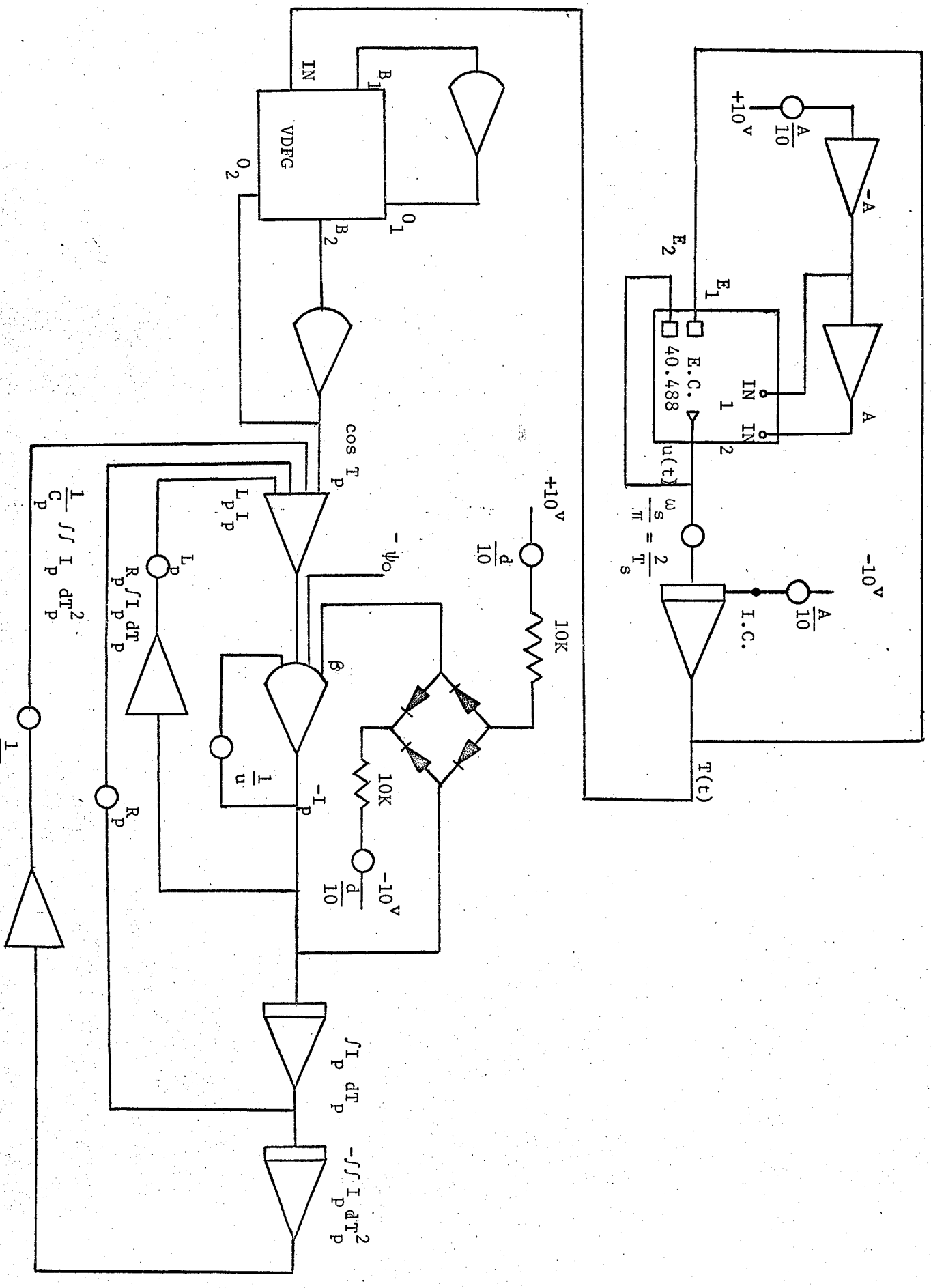

APPENDIX E

NUMERICAL DATA FOR FIGURES

E.1 Data for Figure 5.8, page 54.

series compensations X_c (per unit)	subharmonic currents I_m^+ (per unit)	capacitor voltages $V_{c_{p-p}}$ (per unit)
0	--	--
.0935	--	--
.187	--	--
.281	--	--
.375	--	--
.468	1	.95
.562	.8	.83
.655	.7	.70
.748	1.75	1.5
.795	1.72	1.48
.844	1.55	1.45

E.2 Data For Figure 5.11, page 58.

series compensations X_c (per unit)	subharmonic currents I_m^+ (per unit)	capacitor voltages $V_{c_{p-p}}$ (per unit)
0	--	--
.0935	--	--
.187	--	--
.281	--	--
.375	1.25	1.1
.468	1.05	0.95
.562	0.85	0.90
.655	2.35	1.85
.748	1.90	1.55
.844	1.55	1.44

E.3 Data for Figure 5.12, page 59.

Linear ranges ψ_s (per unit)	subharmonic currents I_m^+ (per unit)
1	1.90
1.2	1.75
1.3	1.70
1.4	0.60
1.5	0.55
1.6	--

BIBLIOGRAPHY

1. Kloeffler, R. G., Kerchner, R. M., and Brenneman, J. L., *"Direct-current Machinery"*, Macmillan Company, New York, 1948, pp. 376 - 388.

2. Thompson, S. P., *"Dynamo Electric Machinery"*, Home Book Company, New York, 1893, pp. 121 - 194.

3. Stevenson, W. D., *"Elements of Power System Analysis"*, McGraw-Hill Book Company, New York, 1962.

4. Knudsen, N. H., *"Abnormal Oscillations in Electric Circuit Containing Capacitor"*, Trans. Roy. Institute, Stockholm, No. 69, 1953.

5. Angello, S. T., *"The Effects of Intitial Conditions on Subharmonic Currents in a Non-linear Series Circuit"*, AIEE, vol. 61, 1942, pp. 625 - 627.

6. Portnoi, M. G., *"The Occurrence of Subharmonic Resonance in Unbalanced Conditions"*, Electro Technology, U.S.S.R., 1959, pp. 589 - 598.

7. Glavitsch, J., *"Power-frequency Overvoltages in EHV Systems"*, Brown Boveri Review, vol. 51, No. 1/2, 1964, pp 21 - 32.

8. West, J. C., and Douce, J. L., *"The Mechanism of Subharmonic Generation in a Feedback System"*, Proc. IEE, vol. 102, 1955, pp 569 - 574.

9. Gibson, J. E., *"Nonlinear Automatic Control"*, McGraw-Hill Book Company, New York, 1963, pp. 342 - 438.

10. McCrumm, J. D., *"An Experimental Investigation of Subharmonic Currents"*, AIEE, vol. 40, 1941, pp. 533 - 540.

11. Nagamura, J., *"Abnormal Phenomena of The Series Capacitor Compensated Systems"*, Technical Report No. 603, Electrotechnical Laboratory (Japan), May 1961, Chapter VII.

12. Boyajian, A., *"Mathematical Analysis of Non-linear Circuits, Part I"*, AIEE, vol. 34, 1931, pp. 531 - 537.

13. Boyajian, A., *"Mathematical Analysis of Non-linear Circuits, Part II"*, AIEE, vol. 34, 1931, pp. 745 - 750.

14. Alden, R. T. H., *"Analysis of Subharmonic Oscillations in a Nonlinear Circuit"*, M.Sc. Thesis, University of Toronto, 1964.

15. Hayashi, C., *"Subharmonic Oscillations in Non-linear Systems"*, Journal of Applied Physics, 1953, pp. 521 - 529.

16. Achsaf, C., *"On the Derivation of the Describing Function for Hysteretic Non-linear Elements"*, M.Sc. Thesis, University of Manitoba, 1965.

17. Wylie, C. R., *"Advanced Engineering Mathematics"*, McGraw-Hill Book Company, New York, 1962.

18. Suits, C. G., *"Studies in Non-linear Circuits"*, AIEE, vol. 30, 1931, pp. 724 - 736.

19. Travis, I., *"per-Unit Quantities"*, AIEE, vol. 56, 1937, pp. 22 - 28, of Supplement.

20. Edlinger, A., Glavitsch, H., and Ritter, A., *"The Use of H.V. Reactors for the Compensation of EHV Transmission Lines"*, CIGRE, vol. III, 1964, Report No. 402.

21. Travis, I., and Weygandth, C. N., *"Subharmonics in Circuits Containing Iron-core Reactors, Part I"*, AIEE, vol. 57, 1938, pp. 423 - 431.

22. Travis, I., and Weygandt, C. N., *"Subharmonics in Circuits Containing Iron-core Reactors, Part II"*, AIEE, vol. 58, 1939, pp. 735 - 742.

23. Rudenbergh, R., *"Non-linear Oscillations Caused by Magnetic Saturation"*, AIEE, vol. 68, 1949, pp. 676 - 685.

24. Concordia, C., and Butler, J. W., *"Analysis of Series Capacitor Application Problems"*, AIEE, vol. 56, 1937, pp. 975 - 988.

25. Concordia, C., Kron, G., and Bodine, R. B., *"Self-excited Oscillations of Capacitor-Compensated Long-Distance Transmission Systems"*, AIEE, vol. 62, 1943, pp. 41 - 44.

26. Spitzer, C. F., *"Sustained Subharmonic Response in Non-linear Series Circuits"*, Journal of Applied Physics, 1945, pp. 105.

27. Bessonov, L. A., *"Achievement in the Study of Non-linear Circuits"*, Electro Technology, U.S.S.R., 1963, pp. 100 - 118.

28. Fleishman, B. A., *"Harmonic and Subharmonic Responses of an On-Off Control System to Sinusoidal Inputs"*, Franklin Institute Journal, 1960, pp. 99 - 111.

29. Ludeke, C. L., *"An Electro-Mechanical Device for Solving Non-linear Differential Equations"*, Journal of Applied Physics, 1949, pp. 600 - 607.

30. Ludeke, C. L., *"Predominantly Subharmonic Oscillations"*, Journal of Applied Physics, 1951, pp. 1321 - 1326.

31. DuBois, E. W., *"Extra-Long-Distance Transmission"*, IEEE, vol. 80, 1962, pp. 1108 - 1112.